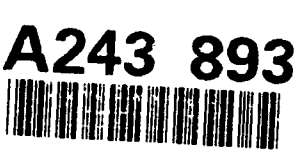



AFIT/GEP/ENP/91D-1



# LOW TEMPERATURE PHOTOLUMINESCENCE STUDY OF SILICON-GERMANIUM ALLOY SUPERLATTICES

THESIS

Maxwell M. Chi
Captain, USAF

AFIT/GEP/ENP/91D-1



# REPORT DOCUMENTATION PAGE

*Form Approved*
*OMB No. 0704-0188*



| 1. AGENCY USE ONLY *(Leave blank)* | 2. REPORT DATE | 3. REPORT TYPE AND DATES COVERED |
|---|---|---|
| | December 1991 | Master's Thesis |

**4. TITLE AND SUBTITLE**

LOW TEMPERATURE PHOTOLUMINESCENCE STUDY OF SILICON-GERMANIUM ALLOY SUPERLATTICES

**5. FUNDING NUMBERS**

**6. AUTHOR(S)**

Maxwell M. Chi, Captain, USAF

**7. PERFORMING ORGANIZATION NAME(S) AND ADDRESS(ES)**

Air Force Institute of Technology,
WPAFB OH 45433-6583

**8. PERFORMING ORGANIZATION REPORT NUMBER**

AFIT/GEP/ENP/91D-1

**9. SPONSORING/MONITORING AGENCY NAME(S) AND ADDRESS(ES)**

LT COL GERNOT S. POMRENKE
AFOSR/NE
BOLLING AFB DC 20332-6448

**10. SPONSORING/MONITORING AGENCY REPORT NUMBER**

**11. SUPPLEMENTARY NOTES**

**12a. DISTRIBUTION/AVAILABILITY STATEMENT**

Approved for public release;
distribution unlimited

**12b. DISTRIBUTION CODE**

**13. ABSTRACT** *(Maximum 200 words)*

Low temperature photoluminescence studies were performed on nine silicon-germanium alloy superlattice samples. The luminescence spectra showed sharp peaks in the 0.95 to 1.05 eV energy range, and a broad band located 0.05 to 0.12 eV below the alloy bandgap. The sharp peaks were identified as transitions associated with impurity-bound excitons. The linewidth was about 10 times that in pure silicon; in addition, the peaks shifted to lower energy as the sample temperature was raised from 1.4 to 15 K. These features were attributed to effects of random distribution of atoms in the alloy. The broad band shifted to lower energy as the temperature was raised and also narrowed considerably in bandwidth. This broad luminescence was attributed to recombination of excitons confined in potential wells created by local fluctuations in the alloy composition.

**14. SUBJECT TERMS**

Photoluminescence; Superlattices; Silicon Alloys; Silicon-Germanium Alloys; Excitons, Thesis

**15. NUMBER OF PAGES**

120

**16. PRICE CODE**

| 17. SECURITY CLASSIFICATION OF REPORT | 18. SECURITY CLASSIFICATION OF THIS PAGE | 19. SECURITY CLASSIFICATION OF ABSTRACT | 20. LIMITATION OF ABSTRACT |
|---|---|---|---|
| Unclassified | Unclassified | Unclassified | UL |

## GENERAL INSTRUCTIONS FOR COMPLETING SF 298

The Report Documentation Page (RDP) is used in announcing and cataloging reports. It is important that this information be consistent with the rest of the report, particularly the cover and title page. Instructions for filling in each block of the form follow. It is important to ***stay within the lines*** to meet ***optical scanning requirements***.

**Block 1.** Agency Use Only *(Leave blank)*.

**Block 2.** Report Date. Full publication date including day, month, and year, if available (e.g. 1 Jan 88). Must cite at least the year.

**Block 3.** Type of Report and Dates Covered. State whether report is interim, final, etc. If applicable, enter inclusive report dates (e.g. 10 Jun 87 - 30 Jun 88).

**Block 4.** Title and Subtitle. A title is taken from the part of the report that provides the most meaningful and complete information. When a report is prepared in more than one volume, repeat the primary title, add volume number, and include subtitle for the specific volume. On classified documents enter the title classification in parentheses.

**Block 5.** Funding Numbers. To include contract and grant numbers; may include program element number(s), project number(s), task number(s), and work unit number(s). Use the following labels:

| | | | |
|---|---|---|---|
| **C** | - Contract | **PR** | - Project |
| **G** | - Grant | **TA** | - Task |
| **PE** | - Program Element | **WU** | - Work Unit Accession No. |

**Block 6.** Author(s). Name(s) of person(s) responsible for writing the report, performing the research, or credited with the content of the report. If editor or compiler, this should follow the name(s).

**Block 7.** Performing Organization Name(s) and Address(es). Self-explanatory.

**Block 8.** Performing Organization Report Number. Enter the unique alphanumeric report number(s) assigned by the organization performing the report.

**Block 9.** Sponsoring/Monitoring Agency Name(s) and Address(es). Self-explanatory.

**Block 10.** Sponsoring/Monitoring Agency Report Number. *(If known)*

**Block 11.** Supplementary Notes. Enter information not included elsewhere such as: Prepared in cooperation with...; Trans. of...; To be published in.... When a report is revised, include a statement whether the new report supersedes or supplements the older report.

**Block 12a.** Distribution/Availability Statement. Denotes public availability or limitations. Cite any availability to the public. Enter additional limitations or special markings in all capitals (e.g. NOFORN, REL, ITAR).

- **DOD** - See DoDD 5230.24, "Distribution Statements on Technical Documents."
- **DOE** - See authorities.
- **NASA** - See Handbook NHB 2200.2.
- **NTIS** - Leave blank.

**Block 12b.** Distribution Code.

- **DOD** - Leave blank.
- **DOE** - Enter DOE distribution categories from the Standard Distribution for Unclassified Scientific and Technical Reports.
- **NASA** - Leave blank.
- **NTIS** - Leave blank.

**Block 13.** Abstract. Include a brief *(Maximum 200 words)* factual summary of the most significant information contained in the report.

**Block 14.** Subject Terms. Keywords or phrases identifying major subjects in the report.

**Block 15.** Number of Pages. Enter the total number of pages.

**Block 16.** Price Code. Enter appropriate price code *(NTIS only)*.

**Blocks 17. - 19.** Security Classifications. Self-explanatory. Enter U S. Security Classification in accordance with U.S. Security Regulations (i.e., UNCLASSIFIED). If form contains classified information, stamp classification on the top and bottom of the page.

**Block 20.** Limitation of Abstract. This block must be completed to assign a limitation to the abstract. Enter either UL (unlimited) or SAR (same as report). An entry in this block is necessary if the abstract is to be limited. If blank, the abstract is assumed to be unlimited.

## Acknowledgments

I wish to thank Profs. Y.K. Yeo and R.L. Hengehold, my thesis advisors, for their guidance throughout the eighteen-month program. I want to especially thank Todd Steiner, for providing abundant and invaluable reading material and discussions, for his patient instruction on the use of the equipment, and for providing many helpful comments on the draft of this thesis. Additionally, I am very grateful to: David Godbey of the Naval Research Laboratory for providing the superlattice samples; José Colon for generous assistance in making the power dependence and decay time measurements; Dave Elsaesser for preparing some of the samples; and Greg Smith, Rick Patton, and Leroy Cannon for keeping the laboratory equipment operating smoothly. I also owe a debt of gratitude to all of the countless physics students who preceded me, for maintaining the equipment in fine working condition.

Most of all, I would like to thank my new wife Caroline, for her understanding and support over the last six months.

Maxwell M. Chi

## Table of Contents

List of Figures

List of Figures cont'd

List of Figures cont'd

List of Tables

List of Tables cont'd

## Abstract

Low temperature photoluminescence studies were performed on undoped silicon-germanium alloy superlattices. Three samples showed sharp, intense luminescence peaks in the 0.95 to 1.05 eV energy range. From the positions and temperature dependence of the peaks, they are identified as transitions associated with impurity-bound excitons: the no-phonon transition, and Si and Ge phonon replicas. The binding energy was found from the temperature dependence of the no-phonon line to be about 5 meV, which is the same as in pure Si and in bulk alloys. The no-phonon linewidth was about 10 times of that in pure Si. In addition, the peak shifted by about 5 meV lower in energy as the temperature was raised from 1.4 to 15 K. These features are attributed to effects of the random distribution of atoms in the alloy and local fluctuations in the Ge concentration.

The broad luminescence varied in energy position depending on the alloy bandgap and well width. The peak was 50 to 120 meV below the bandgap. Although wide at low temperatures, as the temperature was raised above 20 K it narrowed considerably and also shifted to lower energy. In addition, as the excitation power was increased it showed first a linear then a sublinear intensity increase. The peak was attributed to recombination of excitons bound to local fluctuations in the alloy composition, because its features could not be entirely explained by other transitions and because it was similar to peaks attributed to fluctuation-bound excitons in other materials.

# I. Introduction

A superlattice is a collection of two or more different materials, arranged in alternating, thin layers such that it demonstrates quantum effects and properties that are strikingly different from its composition materials. The idea of the superlattice was first proposed in 1969[1:1] and the first superlattices were constructed in the 1970s of GaAs. Later, the development of molecular beam epitaxy as a fabrication technique made possible the production of high-quality superlattices made of other materials, including Si and Ge. Si-Ge superlattices have been under experimental study mainly since the mid-1980s.

Superlattices stimulate intense interest not only because of their unique physical properties but also because those properties have potentially important applications in fields such as optical detection and electronics. For example, superlattices could enable Si photodetectors to operate in the near-infrared wavelength band. This would reduce the integration costs of connecting Si integrated circuits to GaAs detectors. The potential savings would be tens of millions of dollars annually[2:463;31:294]. Meanwhile, the already-developed high electron mobility transistor is much faster than the GaAs field effect transistor and has potential use in supercomputers[3:103].

Developing devices based on the superlattice requires thorough understanding of its characteristics. Because the superlattice is so new, much basic research remains to be performed. Considerable theoretical work on the expected

properties and behavior of superlattices has already been done. Experimental efforts are directed toward verifying these calculations as well as generally characterizing superlattice properties and behavior. Some of the active research areas are:

(1) Strained-alloy properties. Because Si and Ge lattices have different crystal cell widths, or lattice parameters, growth of a $Si_{1-x}Ge_x$ epitaxial layer on top of a pure Si or Ge substrate results in strain. This strain has been shown to produce new optical and electronic properties in the alloy, including altered electron energy bands and mobility enhancement[11]. However, not all of the predicted properties have been unambiguously observed.

(2) Quantum effects. When superlattice layers are made sufficiently thin, i.e. less than 100 angstroms thick, quantum effects are seen. The ultrathin layers of material, with alternating wider and narrower bandgaps, act as classical quantum wells for the charge carriers within them. This results in electronic properties that are somewhat different from bulk materials. For instance, the charge carriers have quantized energy states, so that some transitions are shifted to higher energies than in bulk materials[54:717-719].

(3) Quasi-direct bandgap. The Si-Ge superlattice is expected to possess a quasi-direct energy bandgap, even though its component elements are indirect bandgap materials[56;57]. This is a most significant predicted feature of Si-Ge superlattices and has important practical applications. The existence of a quasi-direct bandgap has not thus far been experimentally proven.

To study superlattice properties, the technique of photoluminescence is commonly used. This is a nondestructive technique which enables one to study the electron energy bands and levels within a material by collecting the photons emitted during transitions between those levels. By analyzing these photons, one can obtain relatively detailed information on the band structure and charge carrier distribution and how these vary as functions of temperature. Major limitations of photoluminescence are that it provides information only on radiative transitions (those in which a photon is radiated); that the wavelength information is limited by the resolution of the collection equipment; and that no information is provided on the time history of each emission.

The purpose of this project was twofold. First was to examine the near band edge spectra observed from Si-Ge alloy superlattice samples. In particular, the behavior of these peaks were characterized as a function of temperature and proposed explanations given for some of their observed properties.

The second was to characterize and propose an explanation for the broad luminescence band observed from each sample at 50-120 meV below the alloy bandgap. Similar peaks have been reported in published data from a variety of other superlattice samples and their origin is unclear. This peak is of significance because of its potential use in Si-Ge light emitting devices in the near infrared wavelength range[26:1039].

## II. Background and Theory

### Crystal Lattices and Energy Bands

Most solids are crystalline or amorphous. In a single crystal, the atoms composing the material form a regular, periodic array[4:64]. The crystal atoms are arranged in one of a number of shapes. The simplest are the simple cubic, body-centered cubic, and face-centered cubic (fcc). Si and Ge crystallize in the diamond structure, which consists of two interpenetrating fcc lattices, one displaced along the main diagonal of the cube by one-fourth the length of the diagonal. Fig. 1a shows one unit cell of the diamond structure. As one can see, each atom is bound to four others by covalent bonds. Fig. 1b shows a common two-dimensional representation of the diamond structure, with the four bonds drawn as if they were at 90 degree angles.

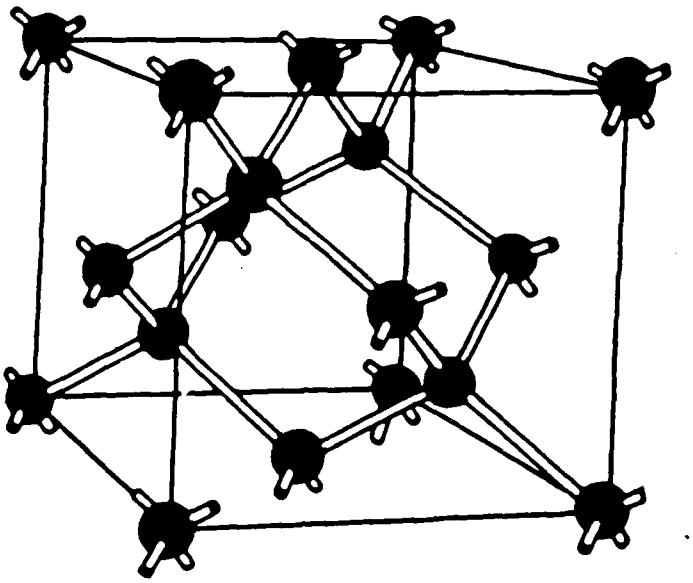

(a)

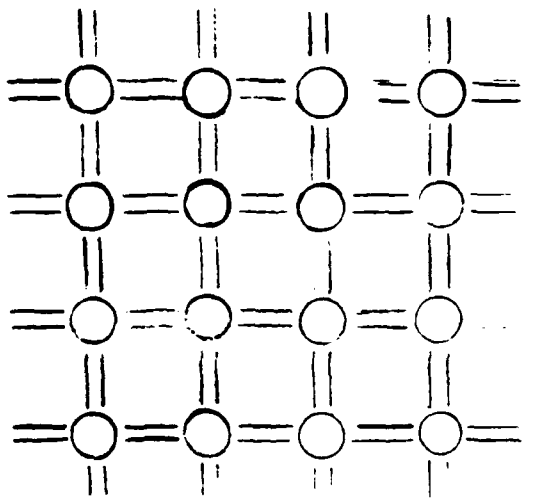

(b)

Fig. 1. Diamond Structure. (a) Three-dimensional structure[54:148]. (b) Two-dimensional representation.

Placing atoms in close proximity, like they are in a crystal lattice, causes electron energy bands to form. An isolated atom has discrete electron energy states. When several such atoms are placed in close proximity, the Pauli exclusion principle requires that the corresponding levels of the different atoms be separated slightly in energy. When many atoms are put together, as they are in a solid, each atomic energy level broadens into a quasicontinuous band. Each of these bands contains a certain number of allowed electron states, and there exists a gap, or forbidden region, between each pair of bands which contains no electron states. Electrons occupy these bands in order, starting with the lowest in energy and proceeding upward. Fig. 2 illustrates atomic energy levels that are broadened into bands as the interatomic spacing decreases. These energy bands are the basis for the distinction between conductors, semiconductors, and insulators. Depending on the number of electrons in the material, the highest band may be either completely or partly filled. An insulator has a completely filled topmost band, as well as a large gap to the next band. Since all occupied bands are completely filled, electrons are not free to move, and thus the material does not conduct significantly. A good conductor has the uppermost band only partly filled, so that electrons in this band are free to move. A semiconductor has the top band filled, but has only a narrow gap to the next band. At very low

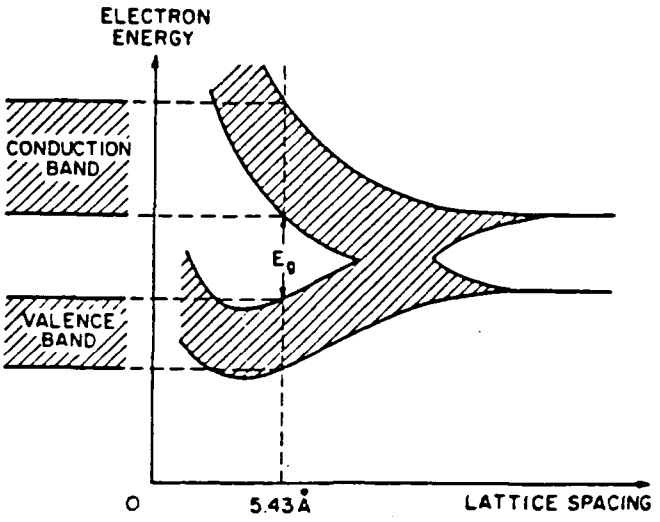


Fig. 2. Electron Band Structures of Elemental Semiconductors

temperature all electrons are in the filled band, called the valence band, and the material does not conduct. At higher temperatures, relatively many electrons thermally excite to the next, empty band, called the conduction band, and the material does conduct. Si and Ge are examples of semiconductors.

Optical Transitions

Band theory is also the basis for understanding optical transitions in a material. When an electron absorbs energy, such as a photon or thermal energy, it jumps from the valence to the conduction band. As it jumps, it leaves a vacant electron state behind. This empty state is called a hole and acts like a positive charge. After a short time, the electron drops back from the conduction band to a state in the valence band,

recombining with the hole and sometimes emitting a photon in the process.

This so-called band-to-band transition is not the only one possible, however, and in fact is quite unlikely to occur in an actual crystal. An electron and hole experience Coulomb attraction and in a crystal can form a single unit, called an exciton, which moves freely throughout the lattice. When an electron and hole form an exciton, the electron actually occupies energy states just below the conduction band. If the "ground state" of the crystal has all electrons in the valence band, then these energy levels represent the "excited states" of the crystal, hence the name exciton[5:74]. One type of transition that occurs frequently in real crystals is exciton recombination, in which an electron in an exciton level recombines with a hole in the valence band. The transition may be either direct or indirect, depending on the material. In direct bandgap materials, the exciton can recombine with no other atoms participating. In indirect bandgap materials, such as Si and Ge, the transition must be accompanied by emission of a phonon, a quantum of atomic lattice vibration, to conserve momentum. The exciton states, along with recombination transitions, are shown in Fig. 3. Although many exciton levels are pictured, actually only the n=1 and possibly the n=2 level can be occupied before the exciton is ionized.

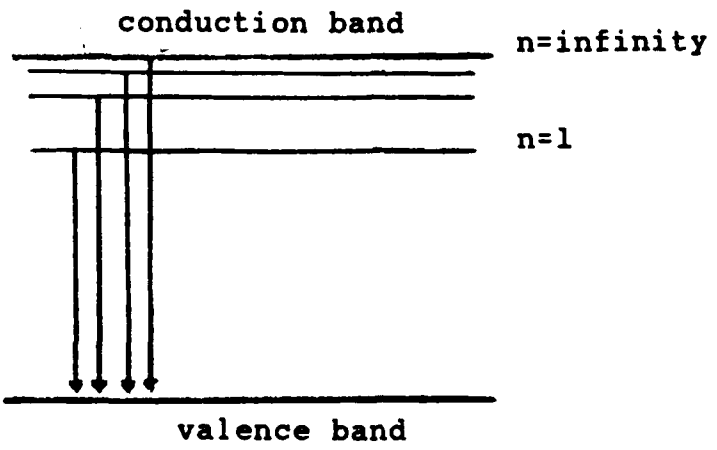


Fig. 3. Exciton Energy Levels

The binding energy of an exciton is approximately[6:12]:

$$E_x = -m^* e^4 / 2\hbar^2 k^2 n^2 \qquad (1)$$

where: $m^*$ is the electron effective mass in the crystal;

$k$ is the dielectric constant of the material; and

$n$ is the number of the exciton energy level.

The forbidden region also contains other energy levels, such as the impurity levels. Even the purest crystals that can be grown today contain some impurities, trace amounts of elements other than the one being grown. The impurity atoms occupy lattice sites that are meant to be filled by atoms of the host material. An impurity concentration as low as a few parts per

billion can affect the crystal's properties[5:46-47]. The effect of impurities is to create extra energy levels in the forbidden region which electrons and holes can occupy. The impurity levels that are created depends on the nature of the impurity. An impurity with a valence greater than the host material is called a donor, since it "donates" one or more electrons. For example, in Si, only four electrons are needed from each atom to fill lattice bonds. An element from Group V in the periodic table will be a donor, since it donates one extra electron. This electron will be loosely bound to the donor and can be easily excited to the conduction band. The extra electron thus occupies an energy level just slightly below the conduction band. Conversely, an element with valence lower than the host material, such as a Group III element in Si, will be an acceptor. Having only three valence electrons, the acceptor will leave one lattice bond empty. We consider the acceptor impurity to have created an

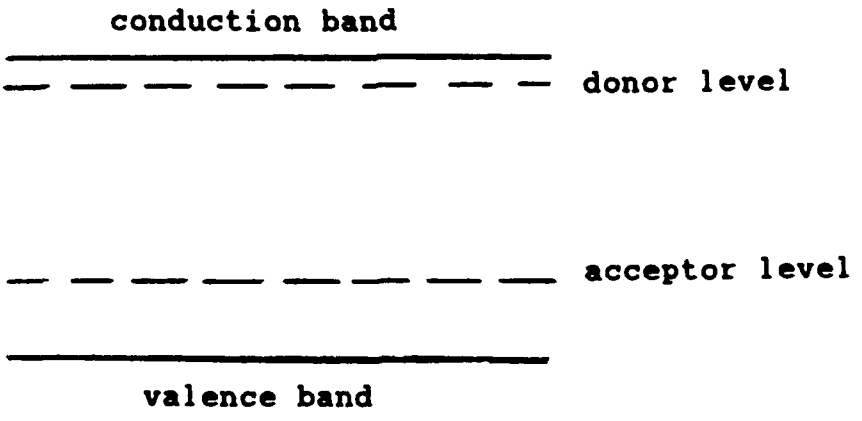


Fig. 4. Donor and Acceptor Energy Levels

acceptor level, just above the valence band, which is filled by a hole. The donor and acceptor levels are illustrated in Fig. 4. The binding energy of the electron or hole to an impurity is very similar in form to the exciton binding energy[7:506]:

$$E_i = -m^* e^4 / 2\hbar^2 k^2 n^2 \qquad (2)$$

where: $m^*$ is the electron or hole effective mass in the crystal;

$k$ is the dielectric constant of the material; and

$n$ is the quantum number of the energy state.

Once the electron or hole is excited to the conduction or valence band, the impurity atom left behind is ionized and becomes charged.

A vacancy can also create bound states in the bandgap. A vacancy is a site where an atom is missing. It can create donor, acceptor, or complex levels.

Impurities and vacancies can bind excitons as well as isolated charge carriers. An ionized, or even a neutral, impurity can attract excitons by Coulomb attraction. The exciton then becomes bound, or "trapped," and as a result its recombination energy is lowered. Particularly in Si and Ge, which are indirect bandgap materials, excitons have a low probability of recombination and therefore are likely to be trapped[8:95].

Excitons can also be trapped by dislocations. When a crystal is subjected to physical stress, part of one crystal plane may slip over another. The boundary between the slipped

and unslipped portions is called a dislocation (Fig. 5). Such dislocations produce unsaturated bonds which can act as traps[5:281].

Photoluminescence and Transition Energies

The technique of photoluminescence (PL) is based on collecting photons emitted when electrons transition from a higher to a lower energy level. PL is typically performed by means of a laser beam irradiating the material. When the incident photons enter the material, electrons absorb their energy and excite to a higher energy level, such as from the

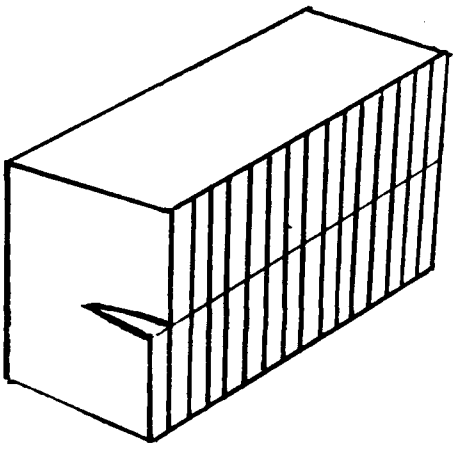

Fig. 5. Dislocation

valence band or impurity levels to the conduction band. When they drop back down to the lower energy states, the electrons give up their energies in one of several ways, including radiating their own photons.

As mentioned previously, the band-to-band transition is relatively unlikely to occur in most materials. More probable are transitions within the bandgap, in particular free and bound exciton recombination, free-to-bound donor, free-to-bound acceptor and donor-to-acceptor transitions. Transitions can also occur that are greater than the bandgap, but these emissions are mostly reabsorbed before they leave the material and are seldom seen. For free exciton recombination, the radiated energy will be

$$E_x = E_g - E_b \tag{3}$$

where $E_g$ is the bandgap energy and $E_b$ the exciton binding energy. For bound exciton recombination, the energy is

$$E_{be} = E_g - E_b - E_{ib} \tag{4}$$

where $E_{ib}$ is the binding energy to the impurity. For the free-to-bound transitions, the emitted photon energy is

$$E_{fb} = E_g - E_i \tag{5}$$

where $E_i$ is the impurity level energy, either donor or acceptor. The donor-to-acceptor transitions involve an electron transferring from an unionized donor to a neutral acceptor. If the donor and acceptor atoms are separated by a distance R they will have a Coulomb energy of $-e^2/4\pi kR$ and the radiated photon energy will be[5:369]

$$E_{da} = E_g - E_d - E_a + e^2/4\pi\kappa R. \quad (6)$$

The above description refers only to direct transitions. Since pure Si and Ge are indirect bandgap materials, in theory all transitions must involve emission of a phonon to conserve momentum. The radiated emission will then be decreased in energy by an amount equal to the phonon energy. But since all real crystals contain some impurities, no-phonon (NP) transitions can occur, in which the impurity atom transfers the momentum. The transition will thus result in an NP emission line at the transition energy along with one or more phonon "replicas," which are shifted to lower energies. In Si at low temperature, most luminescence is from bound exciton recombination. Free carrier and free exciton transitions are very seldom seen[8:102]. The same applies to Ge, since its properties are very similar.

Si-Ge Superlattices

A superlattice (SL) consists of layers of a semiconductor material each of which is "sandwiched" between two layers of a different semiconductor. The two materials have different energy bandgaps, so that the conduction and valence bands in the superlattice are alternately higher and lower, forming a series of potential wells. Fig. 6 shows a typical SL structure and the energy bands that result.

Between the substrate and SL materials is often a buffer layer. The main purpose of the buffer is to insure an atomically flat surface for subsequent growth of the SL. Another purpose is to engineer the lateral lattice constant of the SL. In Si-Ge

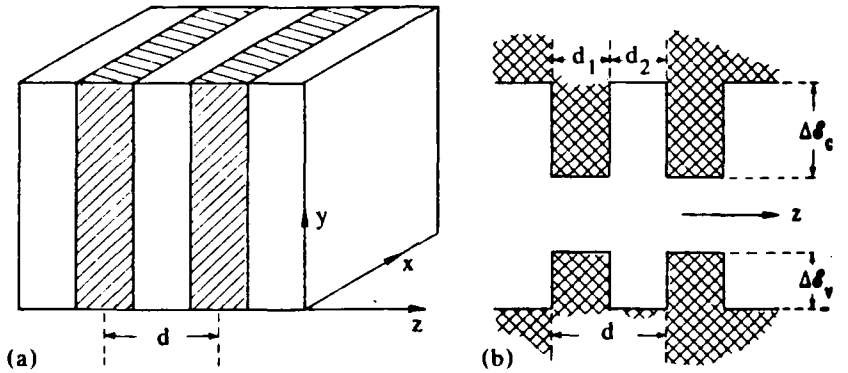


Fig. 6. Superlattice Structure[54:716]. (a) Physical structure. (b) Energy bands.

SLs, the buffer serves an additional purpose[18:132;19:116]. Because the lattice constants of the two materials are different, growing one on top of the other results in strain for both materials. If the total strain is too large, misfit dislocations, or broken lattice bonds, will result and penetrate into the SL, adversely affecting its properties. The buffer is designed to provide a transition between the substrate and SL, such that the lower side is lattice matched to the substrate and the upper side to the SL. The buffer can also improve SL crystal quality by minimizing the penetration of misfit dislocations into the crystal. Dislocations will be largely confined to the interior of the buffer and the interface plane. Although the buffer serves to minimize the strain and penetration into the SL

of dislocations, some strain and dislocations will still remain.

In a Si-Ge or Si/Si-Ge SL, one material is Si while the other is, respectively, Ge or an Si-Ge alloy. The properties of the SL are appreciably different depending on whether pure Ge or an alloy is used. Because all of the SL samples studied in this project involved Si-Ge alloys, this section will concentrate on that type.

The SL structure has three main characteristics that alter the properties of its constituent semiconductor materials. First, the SL's repeated alternating layers of material leads to a "superperiodicity" in the lattice. The SL's fundamental unit cell is Si atomic layers followed by alloy layers, and each of these layers consists of several atomic sublayers of Si or alloy. On the other hand, the lattice unit cell in silicon with the diamond structure is four atomic layers. The SL's unit cell is thus much longer than that of the bulk material. The effect of this superperiodicity is to fold the energy bands into a narrower cell in k-space. Fig. 7 shows a schematic of this effect. This is the basis for predicting a quasi-direct bandgap in a Si-Ge SL. Whereas the original material had an indirect gap, in which the conduction band and valence band edges were separated in k-space, after several foldings resulting from the superperiodicity the SL possesses an almost-direct gap. Zone-folding does not apply to long-period $Si_{1-x}Ge_x$/Si SLs, such as used here.

The second Si/Ge SL feature is strain. The lattice constant, or length of one side of the cubic unit cell, differs

for the two materials by about four percent, with Si at 5.43 angstroms and Ge at 5.65 angstroms. The lattice constant of an $Si_{1-x}Ge_x$ alloy varies linearly between these values depending on the Ge content. Growing an alloy on top of a pure Si substrate

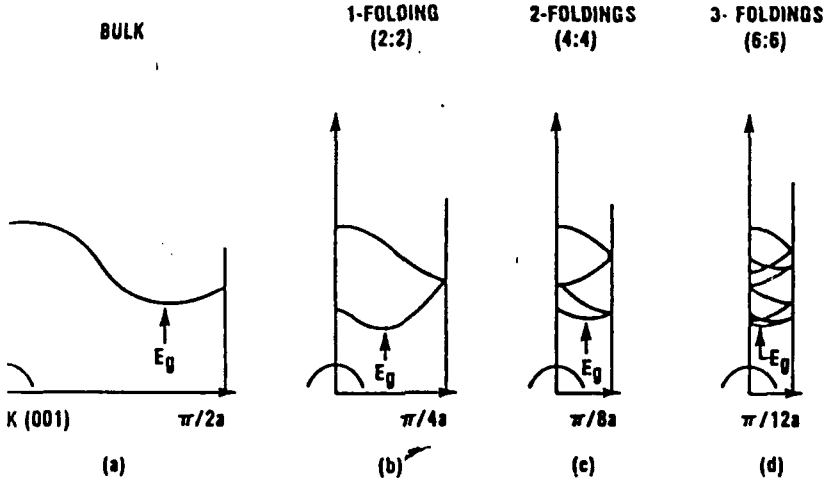


Fig. 7. Energy Band Folding[9:570]

thus results in strain: the Si is stretched and the alloy compressed. Fig. 8 shows a schematic diagram of a strained Si-Ge SL.

The strain affects the energy bands and the transition energies for direct optical transitions. The strain can be separated into two components: compression in the directions parallel to the substrate, which lowers the energy bands in these directions, and tension in the direction perpendicular to the substrate, which raises the energy in that direction. But these directions are the directions of the conduction band energy minima in Si. Thus, the strain lifts the threefold degeneracy of

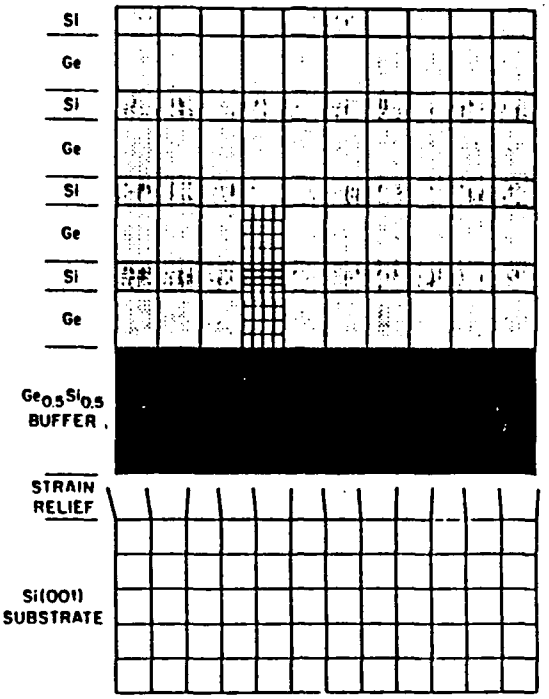


Fig. 8. Strained Si-Ge Superlattice[9:567].

the conduction band, lowering the minimum in some directions and raising it in others[10:131;9:557-8]. The net effect is that, relative to unstrained alloys, the minimum energy bandgap is lowered by up to 0.3 eV, depending on the alloy composition and substrate orientation and composition [11:435]. However, with a Si substrate the energy bands remain Si-like even for high-Ge content alloys[10:132]. For a strained alloy of Ge concentration x, the room-temperature bandgap is given by[9:558]:

$$E_g(x) = 1.1 - 1.02x + 0.52x^2 \quad (6)$$

Fig. 9 shows calculated energy bandgaps for unstrained and strained Si-Ge alloys. The strain also increases the energies of direct optical transitions. As the alloy composition becomes

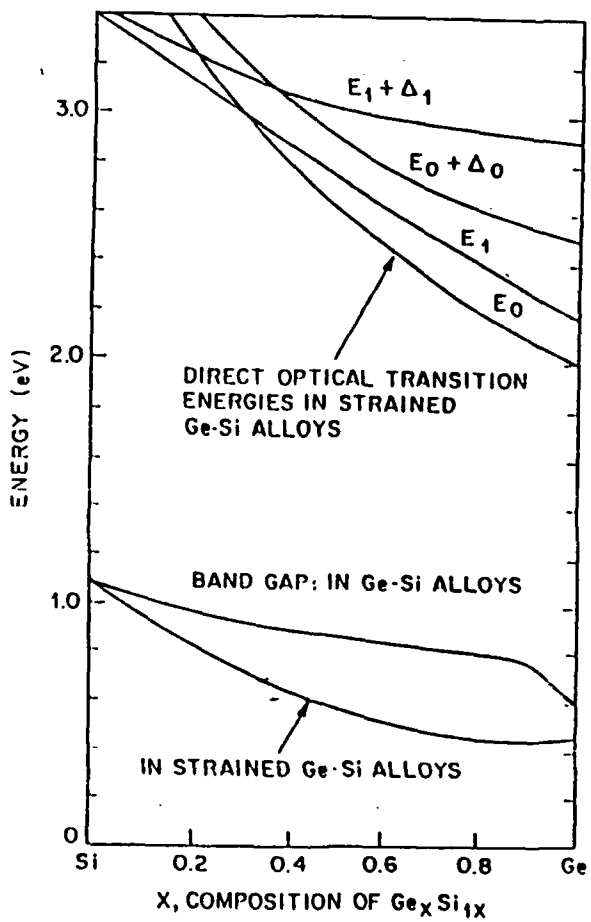


Fig. 9. Strained Alloy Bandgaps and Transition Energies[9:564].

increasingly Ge-rich, the level of strain increases quadratically and so do the transition energies. The transition energy for the $E_0$ transition is[9:562]:

$$E_0 = 4.2 - 4.6x + 2.4x^2 \text{ eV} \quad (7)$$

for an alloy of Ge concentration x.

The strain that results from lattice mismatch limits the thickness of the alloy layer that can be grown. The alloy must accommodate the lattice mismatch by strain, which results in a strain potential energy being stored in the alloy. The thicker the alloy, the more the alloy is strained, and the more strain energy is stored. If the strain energy exceeds a certain critical value, the alloy attempts to "relax" by developing a significant number of "misfit dislocations," or broken bonds which degrade its properties. Therefore, the layers must be kept extremely thin, about 100 angstroms or less, depending on the Ge concentration in the alloy. This became possible in Si-Ge only with the advent of molecular beam epitaxy as a growth technique in the late 1970s[9:552].

The very thin material layers produce the third major characteristic of SLs: quantum effects. The thin, alternating bandgap materials act as potential wells for the electrons and holes within them. The exciton energy levels are very close to the classical particle-in-a-box levels calculated from quantum mechanics, and the exciton transitions correspond to transitions between those confined levels. The transition energy for free exciton recombination is found from[12:70]:

$$E = E_G + E_c^{e,n} + E_c^{h,m} - E_x \quad (8)$$

where $E_G$ is the bandgap energy; $E_c$ is the confinement energy of the electron in its nth level or the hole in its mth; and $E_x$ is

the exciton binding energy. Fig. 10 illustrates SL exciton levels.

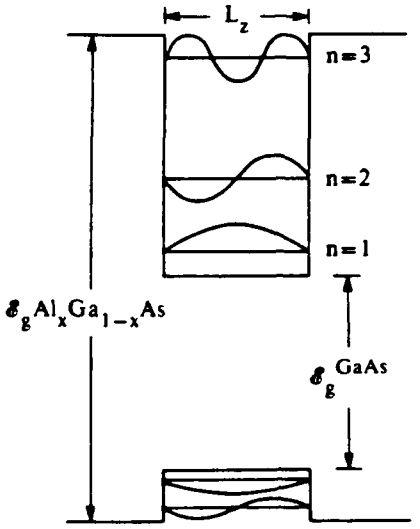


Fig. 10. Superlattice Exciton Energy Levels[54:718].

One often thinks of the SL as lowering the dimensionality of the material: whereas a bulk layer of crystal obviously has three physical dimensions, if the layer thickness is small compared to the length and width, the crystal can be considered two-dimensional.

The quantum confinement of charge carriers has a number of unique effects:

1) It increases the exciton binding energy. Although no calculation has yet been published of exciton binding energies in Si-Ge SLs, in AlGaAs/GaAs SLs the heavy hole exciton binding energy can be increased from 4.2 meV for bulk GaAs to as high as 17 meV for 50 angstrom wells[14:523;12:73]. As shown in Fig. 10,

the exciton levels of the electron and hole are above and below the conduction and valence band edges respectively, whereas in bulk materials they are within the bandgap. Thus the electron and hole energies are more widely separated, which leads to an increase in binding energy.

2) Related to the binding energy increase is a reduction in the exciton Bohr radius, which is the electron-hole orbital radius. This lower Bohr radius means that the electron and hole wave functions overlap more, which leads to a higher effective oscillator strength for electron-hole transitions. The two wave functions not only overlap but they also match better: all electrons and holes in the same subband have the same wave vector in the quantized direction[12:61].

The combination of the binding energy increase and the electron-hole wave function match produces an increase in the absorption coefficient. This leads to highly resolved exciton peaks in absorption spectra for SLs relative to bulk materials [13:265]. For example, in GaAs SLs the integrated absorption peak of an exciton is about 16 times larger than in bulk materials[12:64].

3) The increased overlap of the electron and hole wave functions also leads to a stronger exciton-photon coupling. The electron-hole overlap concentrates the light-matter oscillator strength. The oscillator strength per transition is increased by a factor N/n, where N is the number of unit cells in the crystal and n the number of unit cells in the exciton volume[12:63]. The

lowered dimensionality also produces an increase in effective oscillator strength: in a bulk crystal, the oscillator strength per crystal unit volume is:

$$f = f_{at} \, (1/\pi a_B^3) \qquad (9)$$

where $f_{at} = 2m \; |\langle u_c|n.r|u_v\rangle|^2 / h$

and $\langle u_c|n.r|u_v\rangle$ is the valence band to conduction band matrix element and $a_B$ the exciton Bohr radius. On the other hand, for a thin-layer superlattice, the oscillator strength per unit area is greater:

$$f = f_{at} \, (8/\pi a_B^2) \qquad (10)$$

where $a_B$ is still the bulk value for the Bohr radius[12:64]. The exciton-photon correlation manifests itself in greatly enhanced quantum well peaks as compared to the thicker barrier and buffer layers. This effect has been observed for several different types of semiconductor SLs[12:70]. The well thickness has also been shown to affect the index of refraction of the SL material.

Molecular Beam Epitaxy

An increasingly popular growth technique for SLs is molecular beam epitaxy (MBE). As mentioned previously, MBE is a relatively new technique that made possible production of high-quality Si-Ge SLs. It enables one to grow crystals with purity better than ten parts per billion, excellent uniformity, and high quality majority and minority carrier features. Low growth rates and accurate thickness control are possible. In MBE, a heated substrate is placed in a high-vacuum chamber. Opposite the

substrate are one or more molecular source guns, each of which contains one of the constituent elements or compounds to be grown. Fig. 11 shows a schematic of a typical MBE growth system.

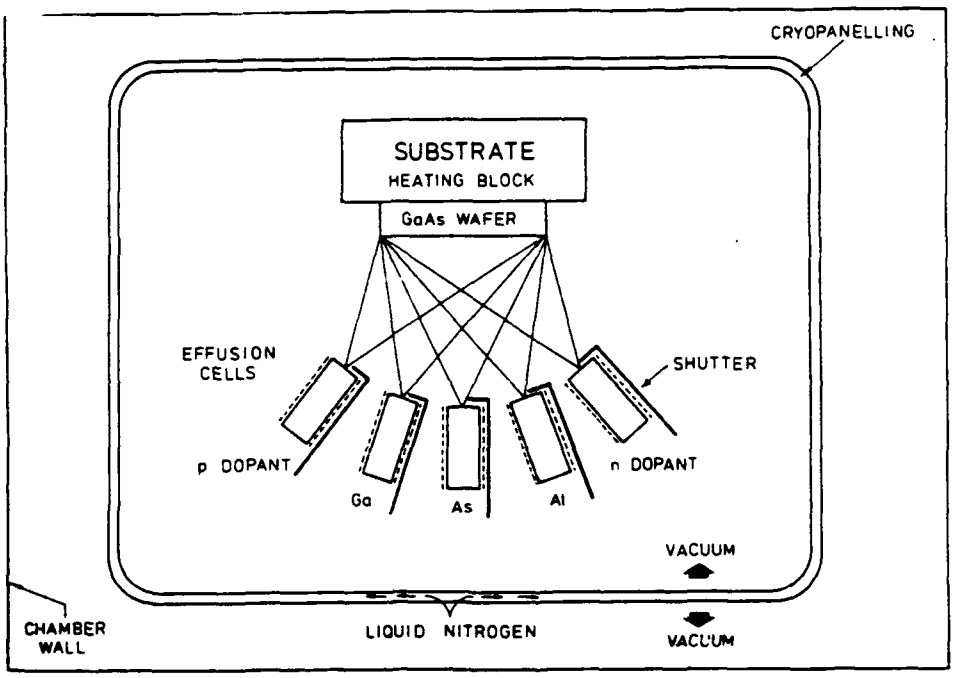


Fig. 11. MBE Growth System[16:17]

The low growth rate of about one micron per hour or one monolayer per second enables one to control the composition or dopant concentration at the atomic level[16:17]. Mechanical shutters control the flow from each gun; thus it is possible for only one gun to irradiate the substrate at a time and one can make different materials grow one on top of another. The substrate is often placed on a plate which rotates in a plane perpendicular to the beam flow. This promotes uniformity in thickness and composition. In addition, masks can be placed over parts of the

substrate to allow more material to be deposited in some locations than others. The vacuum must be extremely high, less than $10^{-10}$ torr. To this end, the MBE system uses low-vapor-pressure materials and liquid nitrogen shields around the high temperature components.

A particularly important consideration in MBE is growth temperature. Growth of silicon at even 80 °C different from the optimum can result in a significant concentration of dislocations and defects. Thus the growth temperature, rate, and pressure must be carefully controlled[17:44].

Annealing

Annealing of SLs may be necessary after growth to reduce concentration of unintentional impurities, defects, or remove radiation damage to the crystal. A relatively new annealing technique was used on the samples in this study and will be described here.

The most notable feature of rapid thermal annealing (RTA) as compared to other methods is short duration. The sample is annealed in 30 to 60 seconds as compared to half an hour in conventional furnace annealing. Since annealing involves both desired physical and chemical processes, such as activation of dopants, and undesired ones, such as displacement of dopant profiles, the advantage of RTA is that it completes the annealing in a short enough time that the unwanted processes are not given a chance to take place[15:60].

In RTA, the sample is continuously kept thermally isolated

and the heating and cooling are done by radiation. Very high heating and cooling rates, in the range 30-500 °C per second can be achieved. Typically, the desired and the undesired processes occur at different activation temperatures. Thus, the advantage of these high heating and cooling rates is that the sample can be maintained at the optimum temperature for the desired process, then quickly cooled so it spends only a fraction of a second at the unwanted process temperatures, much too short for any unwanted process to occur. The undesired processes are almost completely suppressed. For example, annealing is often used on silicon wafers to destroy oxygen donor atoms. Manufacturers conventionally anneal the wafers for 1-2 hours at 600-700 °C. Such long heating times are undesirable because they can produce cracks in large diameter wafers, and also significant clustering of oxygen atoms. On the other hand, RTA at 775 °C for less than five seconds removes over 90 percent of donor atoms, with corresponding increase in conductivity and no significant side effects[15:69].

## III. Previous Work on Si-Ge Superlattices

This section summarizes just a small fraction of previous work on Si-Ge SLs. Although they are relatively new, there is already considerable literature on these structures and the number of publications is growing exponentially every year.

As mentioned in a previous section, Si-Ge SLs have only been produced in significant quantities since the mid-1980s. Consequently, most published work to date has largely consisted of theoretical predictions of Si-Ge SL properties, such as band structure, optical transitions, and charge mobility. Van de Walle and Martin[20] investigated strained interfaces of pure Si and Ge to determine the relative positions of the Si and Ge energy bands, including the discontinuities of the valence band edges. They found a range of 0.27 to 0.75 eV for the valence band discontinuity, depending on the interface. Ting and Chang[21] calculated the conduction band structure of a Si-Ge SL along three different directions. They determined that the bandgap along the [100] direction is quasidirect even though the bulk materials are indirect. This results from the Brillouin zone-folding effect mentioned earlier and from the strain which lowers the conduction band minima in the center of the zone. Finally, Gell[22] calculated transition energies and probabilities for the Si/Ge SL grown on $Si_{1-x}Ge_x$ substrate. He found the crystal stress lowered the symmetry of the lattice in that it produced splittings of previously degenerate states and modified optical selection rules. Band splittings occur at the

zone center and the X zone edge locations. He also confirmed the existence of a quasidirect bandgap and the higher transition probability for bandgap transitions in SLs relative to bulk materials.

On the experimental side, efforts have been largely devoted to characterizing the properties of Si-Ge SLs and comparing them with theoretical predictions. Particular attention has been paid to the quasidirect transition, for this holds the most potential for applications. Okumura et al.[23] reported PL and absorption measurements on five Si-Ge SL samples varying from two Ge and eight Si up to 6 Ge and 24 Si layers per period. They observed PL structure between 750 and 1000 meV consisting of two sharp peaks at 800 and 865 meV and broad shoulders at 850 and 950 meV. This structure they attributed to the SL layer. The strongest peak at 800 meV was about 2 1/2 times stronger than the Si substrate luminescence. The samples were also studied with optical absorption measurements. The absorption coefficient A as a function of wavelength was compared with the relations $A=C_d(hv-Eg)^{1/2} / hv$ which applies to a direct transition; and $A=C_i(hv-Eg)^2$ which is expected for an indirect transition, where $C_d$ and $C_i$ are constants, v the frequency of the incident light, and Eg the bandgap of the sample. The authors interpreted this as evidence of a quasidirect bandgap in Si-Ge SLs.

Similarly, Zachai et al.[24] observed a strong, broad luminescence band centered at about 0.84 eV from an $Si_6Ge_4$ monolayer SL, which they also interpreted as a quasidirect

transition. They noted the peak energy reasonably matched the folded-band direct bandgap transition at the Brillouin zone center calculated from a Kronig-Penney model and given in published calculations. In addition, the peak's strain dependence also agreed with theory. The strongest luminescence came from symmetrically strained samples, and the peak shifted to lower energies with greater strain in the Si layers. The broadening of the signal was caused by strain and thickness fluctuations, which also reduced the transition energies. There is disagreement, however, over the interpretation of these results. Schmid et al.[25] calculated the direct bandgap for Zachai's samples by a different method and arrived at Eg = 1.08 eV. This is 250 meV higher than the luminescence reported by Zachai et al., which Schmid et al. attribute to dislocations in the Si or Ge layers.

A similar, broad luminescence has been reported by other authors in other types of SL samples as well, and its origin is also unknown. Noel et al.[26] reported a broad signal, which they called the strain-localized exciton peak, centered at about 950 meV. Their samples were Si-Ge alloys, but with a long period of 5 nm or more. This ruled out the possibility of Brillouin zone folding and hence a quasidirect transition as the source of the peak. The peak was always about 120 meV below the strained-alloy bandgap and varied almost linearly with the Ge concentration.

Partly because of their weak luminescence, sharp, bound-

exciton (BE) peaks from Si-Ge SLs have been difficult to detect. The first clearly resolved spectra were published earlier this year. Sturm et al.[27] reported no-phonon BE peaks at low temperature and free-exciton peaks at higher temperatures, as well as transverse acoustic (TA) and transverse optic (TO) phonon replicas. The relative positions and linewidths of the peaks matched those from bulk alloys.

## IV. Equipment and Procedure

### Samples

All samples used were grown at and furnished by the Naval Research Laboratory. The samples that the laboratory provided were sections of circular wafers grown by the MBE method briefly described in section II above. From these partial wafers, small rectangular sections about 10 mm by 5 mm were cut for PL study. All samples provided were unannealed; sections of one wafer were annealed and studied in this project. Before each sample was mounted for PL study, it was cleaned to remove surface dirt and contaminants. The recommended cleaning procedure was to spray with trichloroethylene, then methanol and acetone, and finally blow dry with dry nitrogen gas.

### Equipment

Fig. 12 shows a block diagram of the PL equipment used. Each sample was mounted with rubber cement onto a copper mounting block at the bottom of a stainless steel cold finger. The mounting block was lowered into the bottom of the sample chamber where it could be maintained at low temperature. The sample chamber consisted of a Janis Research Model 10DT dewar. Fig. 13 shows a schematic of the dewar setup.

The laboratory procedure was as follows. Before cooling, the jacket between the nitrogen and helium chamber was evacuated with a mechanical rotary pump and a turbomolecular pump. The

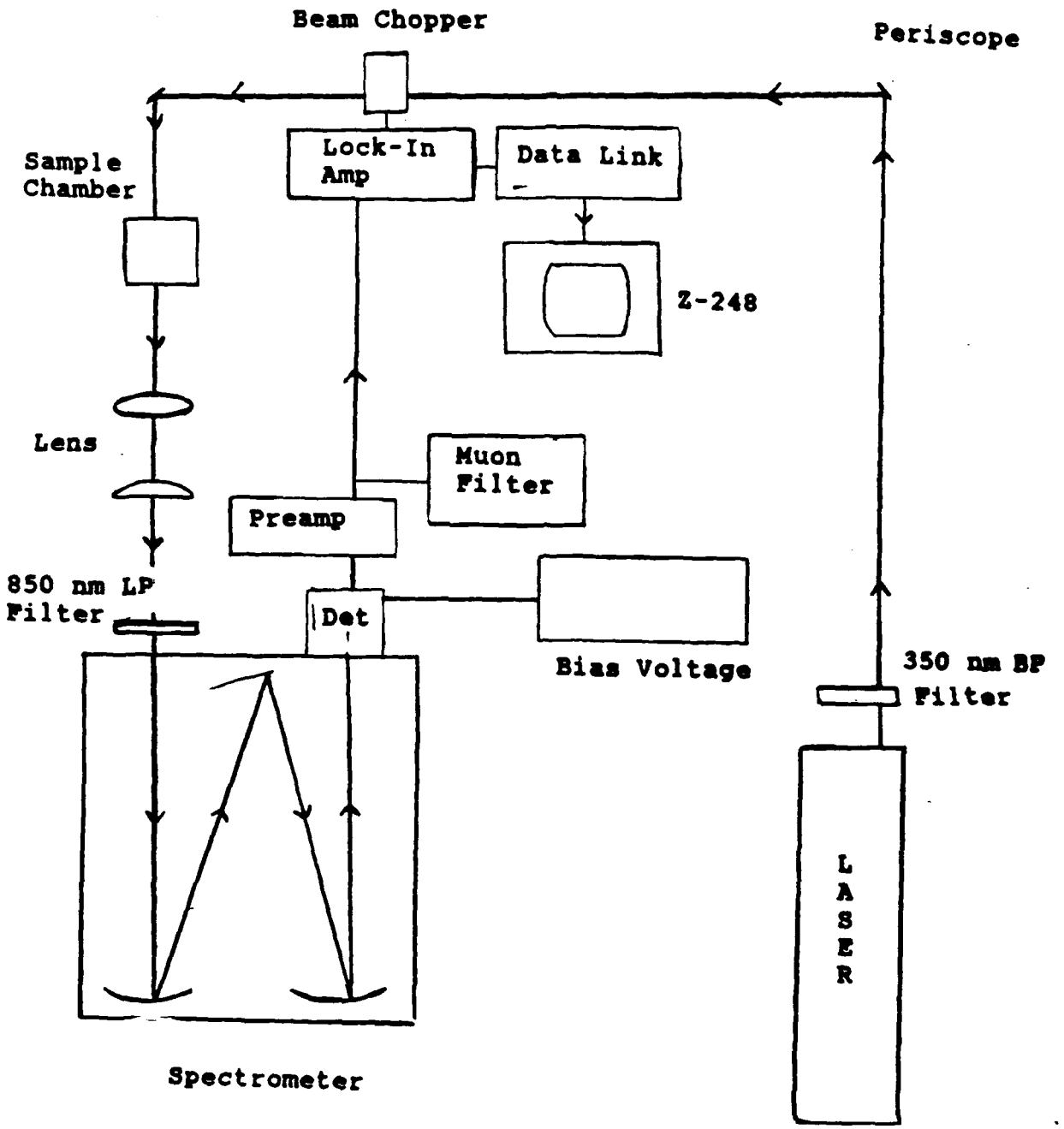


Fig. 12. Photoluminescence Equipment.

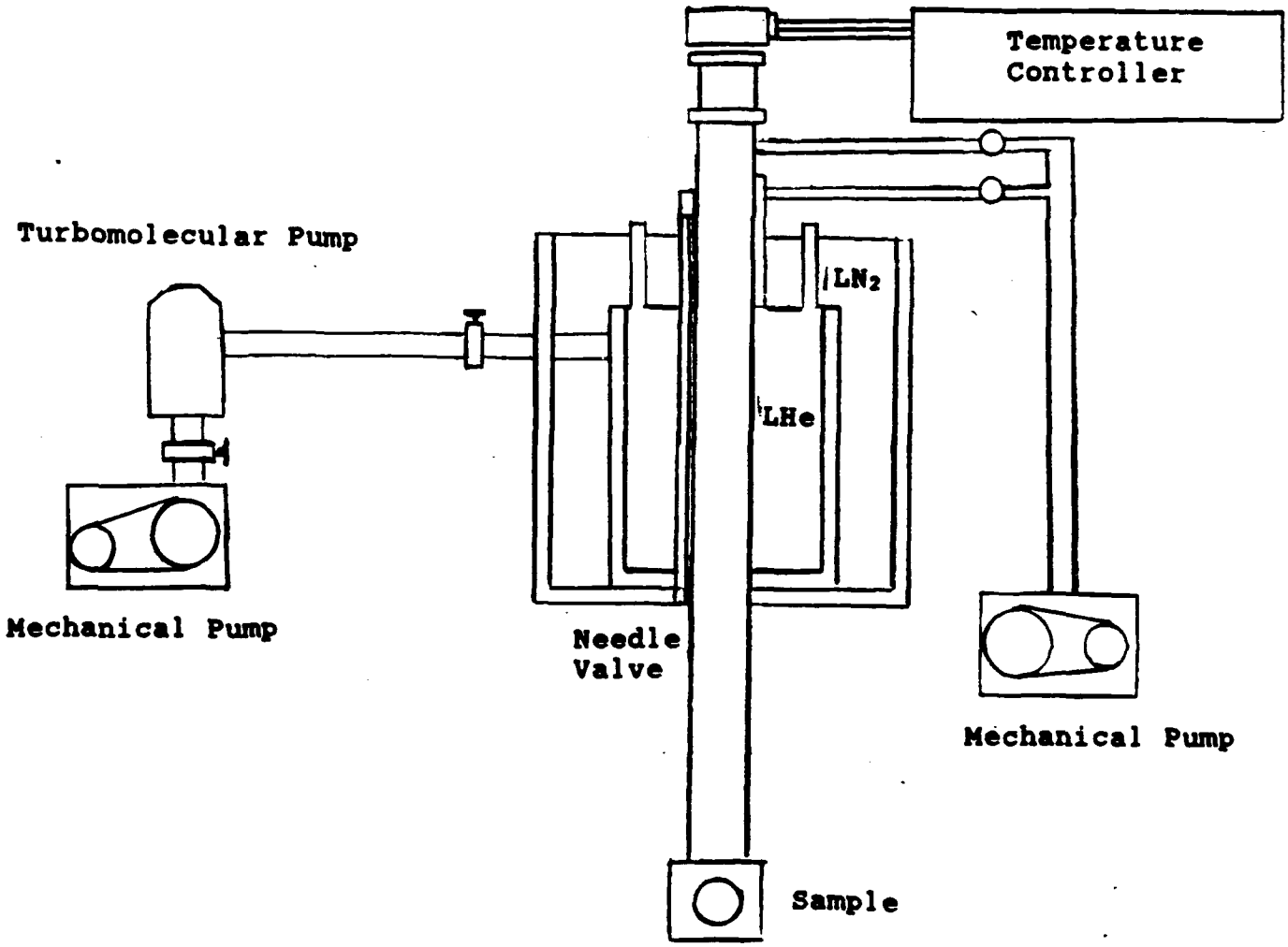


Fig. 13. Sample Chamber Setup.

sample chamber and helium chamber were also pumped to vacuum with a separate rotary pump. The pressure in the jacket was monitored with a micron pressure gauge, and that in the sample chamber with a mercury analog gauge. The helium chamber was pumped for two to four hours before cooling. This was necessary to remove any water vapor and/or other gases in the chamber; if ice formed in the chamber it blocked the flow of liquid helium and caused the needle valve to freeze.

As shown in Fig. 13, both the helium and sample chambers were connected to a mechanical rotary pump. The sample chamber valve was continuously open to pump the sample chamber. The helium chamber valve was open only during the four hours it took to pump the helium chamber. On the other hand, the sample chamber valve was continuously open, except while the sample was being changed. To change the sample, first the sample chamber valve was closed. Then the top of the sample chamber was opened and the cold finger removed. While the sample chamber was open, it was pumped with 2 psi dry helium gas to prevent water vapor from entering the helium chamber. After warming the cold finger, the sample was changed. Finally, the cold finger was reinserted into the sample chamber and the chamber valve again opened.

After pumping of the jacket and helium chamber was complete, the nitrogen chamber was filled with liquid nitrogen. The liquid nitrogen served to cool the equipment to around 90 K. This took about four hours also. The sample temperature was monitored with a Lake Shore Cryogenics model DRC 82C temperature controller.

Finally, the helium chamber was filled to its 15 liter capacity with liquid helium. The flow of liquid He from the helium to the sample chamber was controlled with the needle valve. In addition,the temperature controller provided heating of the sample to maintain it at a desired temperature from 1.4 K to room temperature. To maintain the sample at below 5 K, it was necessary to immerse it completely in liquid He. Unfortunately, this also caused some attenuation of the laser beam and additional noise from liquid He boiling, particularly if the liquid surface was close to the sample.

PL Measurements

The excitation source was a Spectra-Physics model 2020-11 Krypton ion laser which emitted at 350.7 and 356.4 nm. The power range was up to 40 mW. A 350 nm bandpass filter was placed just after the laser to eliminate plasma lines. The beam then reflected off a two-mirror periscope and passed through an optical chopper, controlled by a Stanford Research Systems model SR540 chopper controller. The beam then entered a spectrometer. In front of the spectrometer entrance slit was an 850 nm longpass filter to screen out ambient light and reflection of the laser line. The spectrometer was a SPEX model 1702 3/4 meter Czerny-Turner, blazed at 1.2 microns. The allowed scan rates were 5000, 1000, 250, 100, 50, 25, 5, 1, and .5 angstroms/min. The speed used was 250 angstroms/min. The entrance slit width was usually 1000 or 1500 microns. The exit slit was always set at twice the entrance slit.

From the spectrometer the signal entered a model EO-817L germanium detector, cooled with liquid nitrogen and biased at -250 V with a North Coast Scientific Corp. model 823A bias supply. The signal was amplified with a Stanford Research Systems model SR550 Preamplifier and a Stanford Research Systems SR530 Lock-in Amplifier which was synchronized with the optical chopper frequency. The lock-in/chopper combination served to screen out most extraneous noise in the near-infrared spectrum and prevent it from affecting the signal. The optical chopper was kept at around 45 Hz. The lock-in's time constant was 100 ms. Sensitivity of the lock-in was varied from 500 microvolts to 20 millivolts depending on the strength of the signal. A North Coast Scientific 829B muon filter was used to further eliminate noise spikes from the signal.

The output from the lock-in was fed into a data link and then to a Zenith Z-248 microcomputer. The PL signal was sampled at 15 samples/sec using Labtech Notebook and the spectral data recorded on 3 1/2 inch disk in ASCII format. This format made the data relatively easy to manipulate and display using Quattro Pro, a commercial spreadsheet. The recorded spectra were not calibrated to the spectral response of the system, because it was not required for this project and because the absolute signal intensity was difficult to determine. All spectra are therefore reported in terms of relative intensities. This allows comparison of intensities between different peaks of the same sample, and to a limited extent, between different samples.

The resolution of the spectrometer was estimated using an Ar calibration lamp set in front of the spectrometer. Assuming the calibration lamp lines to have effectively zero linewidth, one can estimate the output signal linewidth and from that the energy resolution in eV. In this way, the spectrometer resolution was estimated to be 3.34 meV at a 1000 micron entrance slit and 5.06 meV at a 1500 micron entrance slit over the energy range recorded.

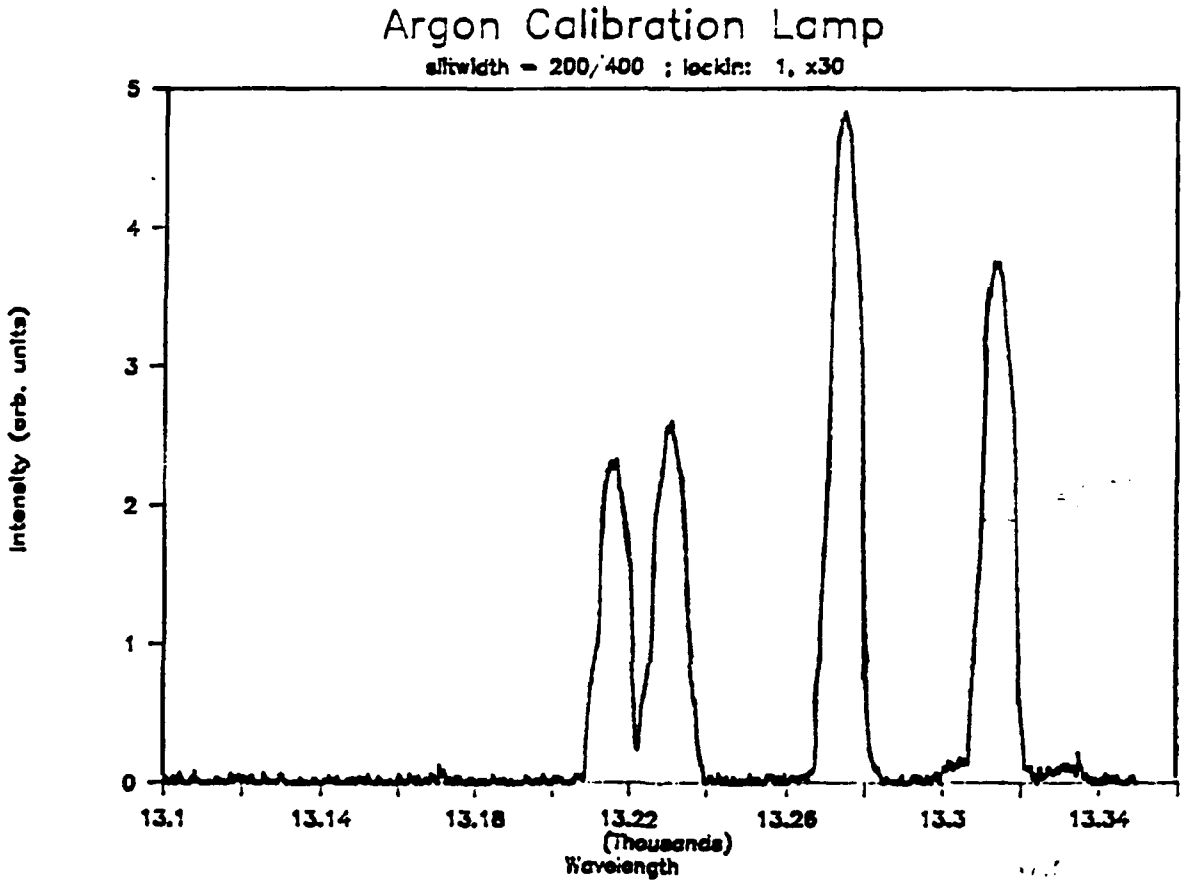


Fig. 14. Argon Calibration Line

# V. Results

## Part 1

All samples used were $Si/Si_{1-x}Ge_x$ SLs. The quantum well structure arises from the difference in bandgap of pure Si, which is 1.17 eV, and an Si-Ge alloy, which varies between 1.17 and .74 eV depending on the Ge concentration. The alloy layers then constituted the wells, and the Si layers, the barriers. All samples had an Si substrate and an Si buffer.

Part 1 of this and the next section concentrate on the narrow, sharp peaks recorded at 0.95 to 1.05 eV.

Fig. 15-17 show PL spectra recorded from three different SL samples. The accompanying tables indicate sample structure and composition. They also indicate the location, intensity, and linewidth (full width at half-maximum) of the peak labelled NP, whose significance is described below.

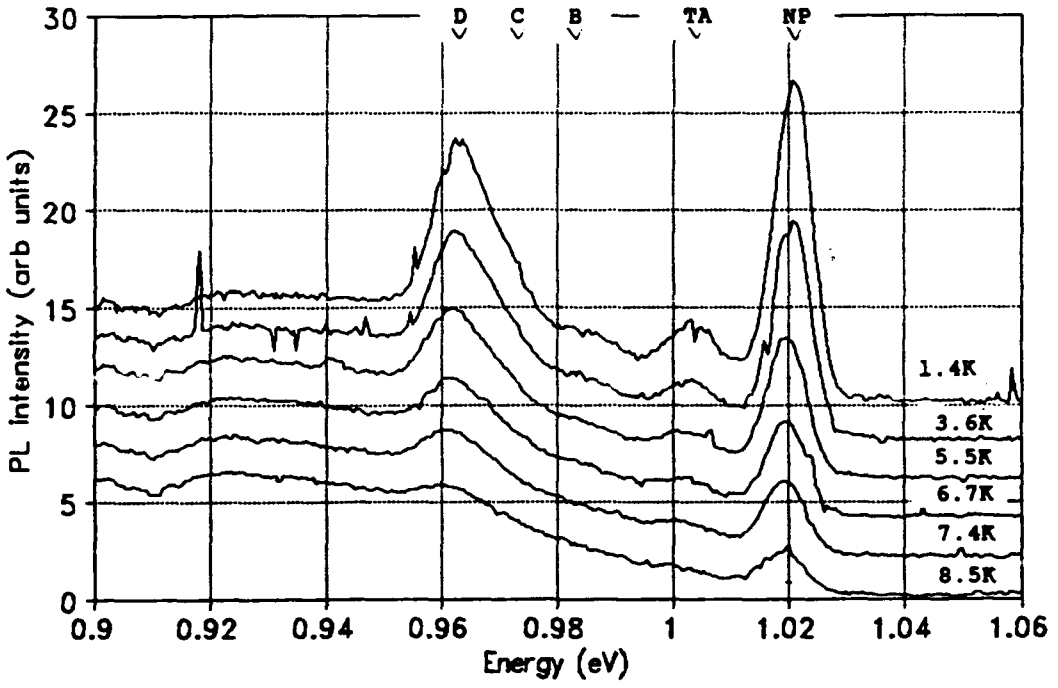


Fig. 15-1. Bound Exciton Spectra of Sample 201.1 at lower temperature

Sample ID: 201.1
Well Width/Barrier Width: 20 angstroms/40 angstroms
Number of Periods: Approx. 80
Nominal Ge Concentration x: 0.25

Table 1
Bound Exciton Spectra of
$Si_{0.75}Ge_{0.25}$(20 Å)/Si(40 Å) sample

| Temp.(K) | Peak Intensity | Peak Position(eV) | Linewidth(eV) | Integrated Intensity |
|---|---|---|---|---|
| 1.4 | 14.90 | 1.0205 | 0.008 | 0.1192 |
| 3.6 | 9.78 | 1.0205 | 0.007 | 0.0685 |
| 5.5 | 5.95 | 1.0195 | 0.008 | 0.0476 |
| 6.7 | 3.85 | 1.0200 | 0.009 | 0.0347 |
| 7.4 | 2.90 | 1.0192 | 0.010 | 0.0290 |
| 8.5 | 1.45 | 1.0192 | 0.011 | 0.0160 |

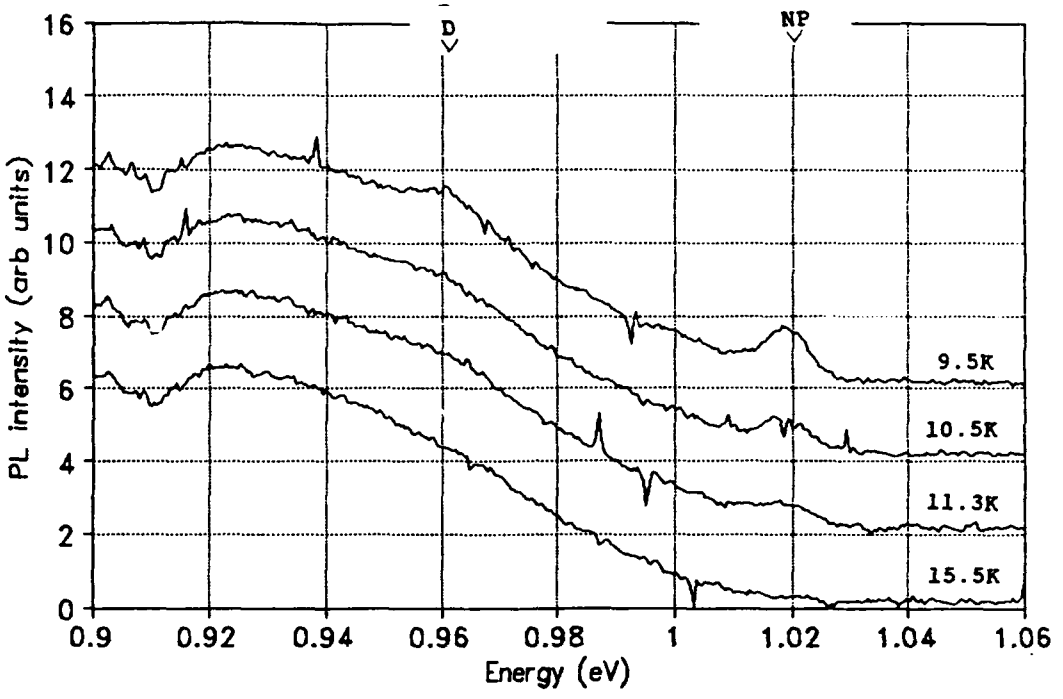


Fig. 15-2. Bound Exciton Spectra of Sample 201.1 at Higher Temperature

Table 1 cont'd

| Temp.(K) | Peak Intensity | Peak Position(eV) | Linewidth(eV) | Integrated Intensity |
|---|---|---|---|---|
| 9.5 | 0.75 | 1.0186 | 0.009 | 0.0068 |
| 10.5 | - | - | - | - |
| 11.3 | - | - | - | - |
| 15.5 | - | - | - | - |

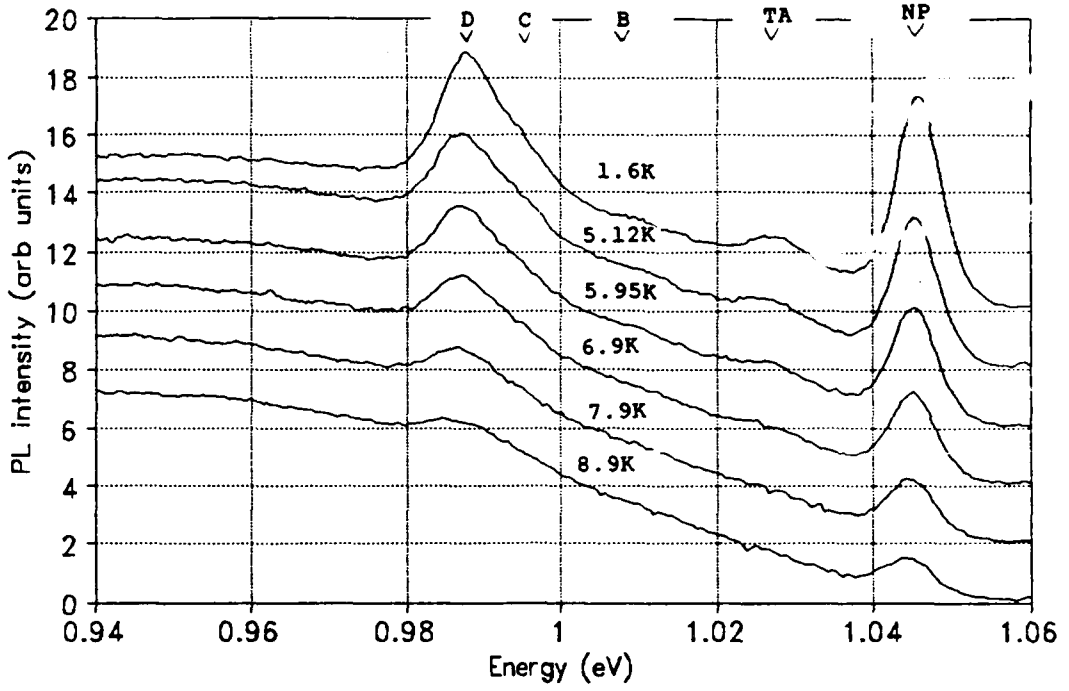


Fig. 16. Bound Exciton Spectra of Sample 206.1

Sample ID: 206.1
Well Width/Barrier Width: 20 angstroms/40 angstroms
Number of Periods: Approx. 80
Nominal Ge Concentration x: 0.25
Annealing: 575°C, 30 sec (RTA)

Table 2
Bound Exciton Spectra of
$Si_{0.75}Ge_{0.25}$(20 Å)/Si(40 Å) sample

| Temp.(K) | Peak Intensity | Peak Position(eV) | Linewidth(eV) | Integrated Intensity |
|---|---|---|---|---|
| 1.6 | 6.45 | 1.046 | 0.0068 | 0.04386 |
| 5.12 | 4.29 | 1.045 | 0.0075 | 0.03218 |
| 5.95 | 3.23 | 1.045 | 0.0072 | 0.02326 |
| 6.9 | 2.39 | 1.045 | 0.0074 | 0.01769 |
| 7.9 | 1.39 | 1.044 | 0.008 | 0.01112 |
| 8.9 | 0.65 | 1.044 | 0.01 | 0.00650 |

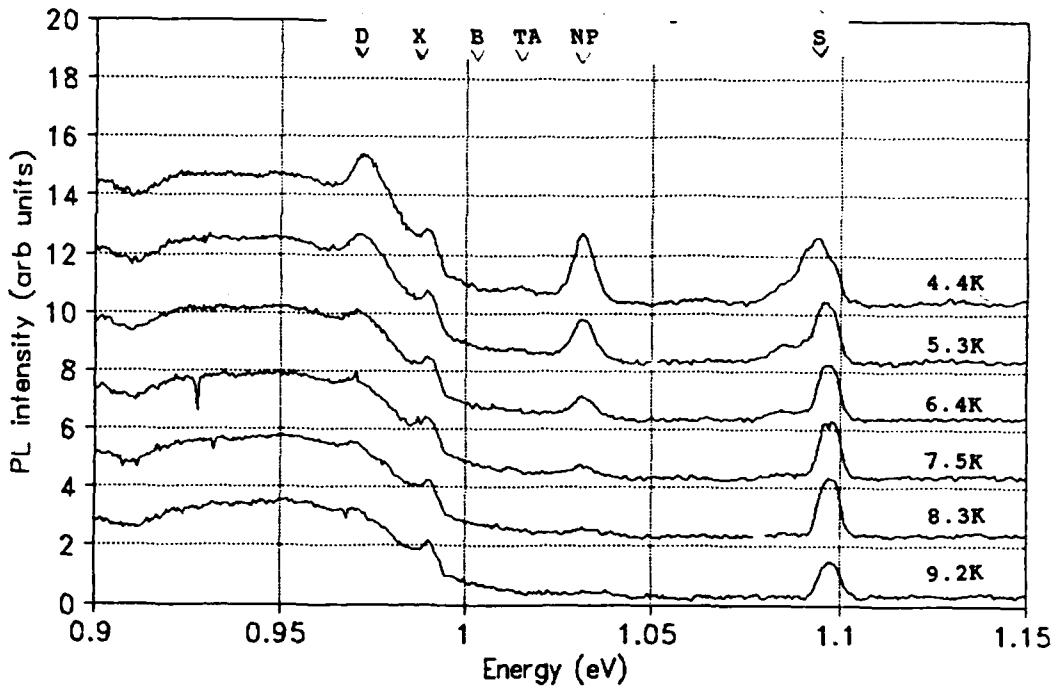


Fig. 17. Bound Exciton Spectra of Sample 10322.2

Sample ID: 1C322.2
Well Width/Barrier Width: 40 angstroms/120 angstroms
Number of Periods: Approx. 30
Nominal Ge Concentration x: 0.25
Annealing: 550°C, 30 sec (RTA)

Table 3
Bound Exciton Spectra of
$Si_{0.75}Ge_{0.25}$(40 Å)/Si(120 Å) sample

| Temp.(K) | Peak Intensity | Peak Position(eV) | Linewidth(eV) | Integrated Intensity |
|---|---|---|---|---|
| 1.6 | 4.375 | 1.032 | 0.0064 | 0.028 |
| 4.4 | 2.39 | 1.032 | 0.0068 | 0.0162 |
| 5.3 | 1.44 | 1.0315 | 0.0071 | 0.0102 |
| 6.4 | 0.80 | 1.031 | 0.0071 | 0.0057 |
| 7.5 | 0.45 | 1.031 | 0.0057 | 0.0026 |
| 8.3 | 0.27 | 1.031 | 0.009 | 0.0024 |
| 9.2 | - | - | - | - |

Part 2

Fig. 18-25 show PL spectra of the BEL luminescence recorded from two of the three samples as above and others. The accompanying tables again show the peak intensity, position, and linewidth.

The W-shaped dip at around 0.9 eV is caused by water absorption, which is predominant at 1.4 microns. Water vapor in the path from the sample to the spectrometer and inside the spectrometer absorbs the luminescence signal.

The detector responsivity drops off sharply below 0.77 eV. This is the cause of the small "kink", or sudden steep drop, at that energy in some of the spectra such as Fig. 19, 22, and 26.

The peak labelled "S" at 1.09 eV in several spectra is luminescence from the substrate. It is believed to be a TO phonon-assisted free exciton plus TO bound exciton transition.

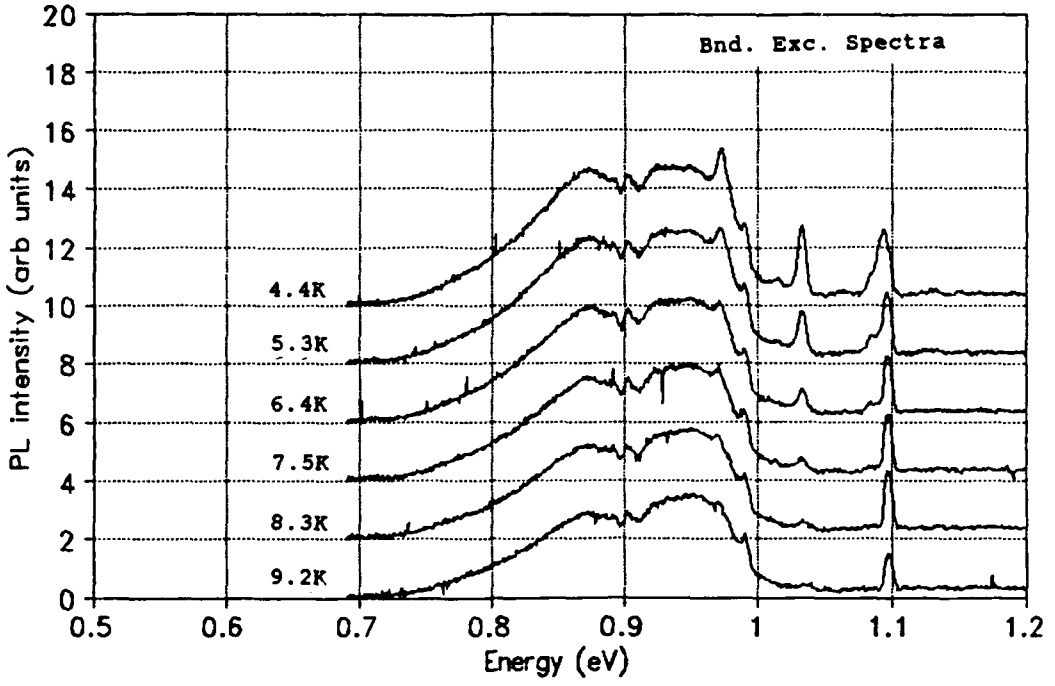


Fig. 18-1. Broad Energy Luminescence Spectra of Sample 10322.2 at lower temperature

Sample ID: 10322.2
Well Width/Barrier Width: 40 angstroms/120 angstroms
Number of Periods: Approx. 30
Nominal Ge Concentration x: 0.25
Annealing: 550°C, 30 sec (RTA)

Table 4
Broad Energy Luminescence Spectra of
$Si_{0.75}Ge_{0.25}$(40 Å)/Si(120 Å) sample

| Temp.(K) | Peak Intensity | Peak Position(eV) | Linewidth(eV) | Integrated Intensity |
|---|---|---|---|---|
| 1.6 | 4.30 | 0.95 | 0.167 | 0.7181 |
| 4.4 | 4.55 | 0.95 | 0.163 | 0.7417 |
| 5.3 | 4.30 | 0.95 | 0.162 | 0.6966 |
| 6.4 | 3.90 | 0.95 | 0.159 | 0.6201 |
| 7.5 | 3.70 | 0.95 | 0.153 | 0.5661 |
| 8.3 | 3.45 | 0.95 | 0.153 | 0.5279 |
| 9.2 | 3.22 | 0.95 | 0.153 | 0.4927 |

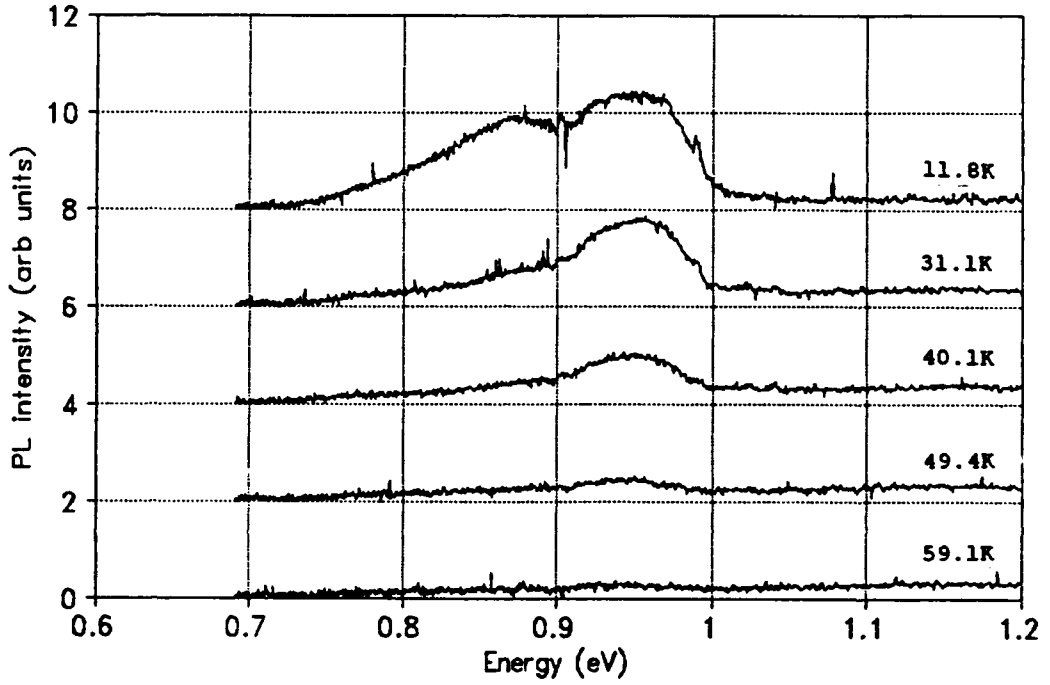


Fig. 18-2. Broad Energy Luminescence Spectra of Sample 10322.2 at higher temperature

Table 4 cont'd

| Temp.(K) | Peak Intensity | Peak Position(eV) | Linewidth(eV) | Integrated Intensity |
|---|---|---|---|---|
| 11.8 | 2.21 | 0.945 | 0.15 | 0.3315 |
| 31.1 | 1.50 | 0.945 | 0.07 | 0.1050 |
| 40.1 | 0.68 | 0.94 | 0.06 | 0.0408 |
| 45.4 | 0.21 | 0.94 | 0.055 | 0.0116 |
| 59.1 | 0.07 | 0.94 | 0.04 | 0.0028 |

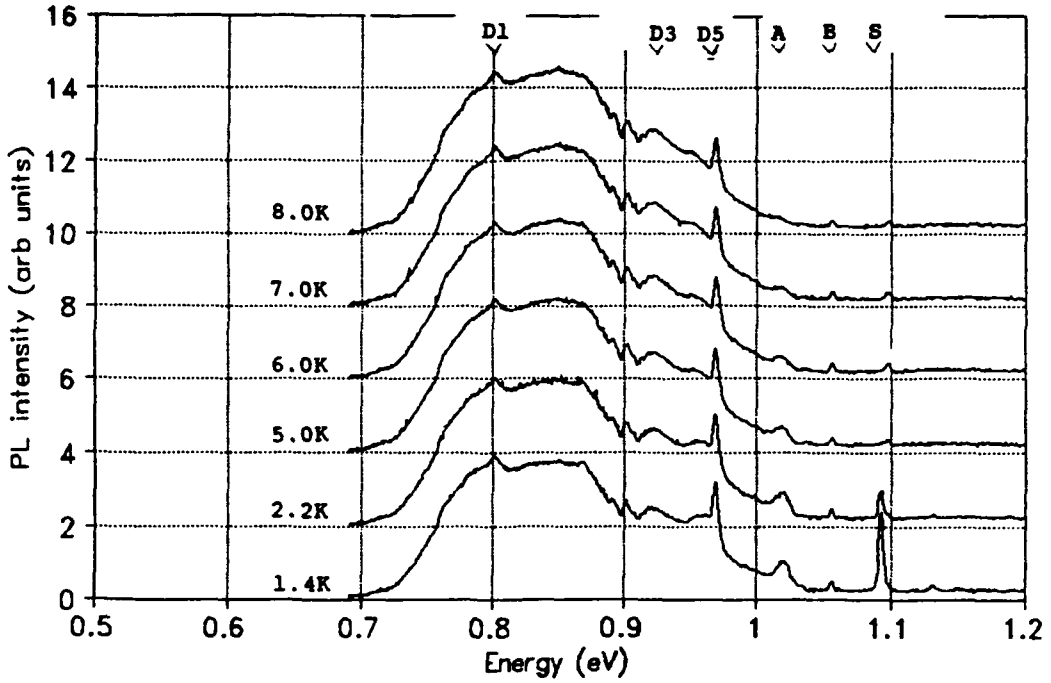


Fig. 19-1. Broad Energy Luminescence Spectra of Sample 201.1 at lower temperature

Sample ID: 201.1
Well Width/Barrier Width: 40 angstroms/20 angstroms
Number of Periods: Approx. 80
Nominal Ge Concentration x: 0.25

Table 5
Broad Energy Luminescence Spectra of
$Si_{0.75}Ge_{0.25}$(20 Å)/Si(40 Å) sample

| Temp.(K) | Peak Intensity | Peak Position(eV) | Linewidth(eV) | Integrated Intensity |
|---|---|---|---|---|
| 1.4 | 6.95 | 0.85 | 0.202 | 1.4039 |
| 2.2 | 7.45 | 0.85 | 0.205 | 1.5273 |
| 5.0 | 7.85 | 0.85 | 0.200 | 1.5700 |
| 6.0 | 8.43 | 0.85 | 0.185 | 1.5596 |
| 7.0 | 8.48 | 0.85 | 0.181 | 1.5349 |
| 8.0 | 8.70 | 0.85 | 0.170 | 1.4790 |
| 9.0 | 7.65 | 0.84 | 0.169 | 1.2929 |
| 10.0 | 7.09 | 0.85 | 0.178 | 1.2620 |

NOTE: These spectra were taken from a different sample than in Part 1.

| | | |
|---|---|---|
| Dislocation Lines: | D1 | = 0.805 eV |
| | D3 | = 0.92 eV |
| | D5 | = 0.97 eV |
| Substrate Lines: | A | = 1.02 eV |
| | B | = 1.055 eV |

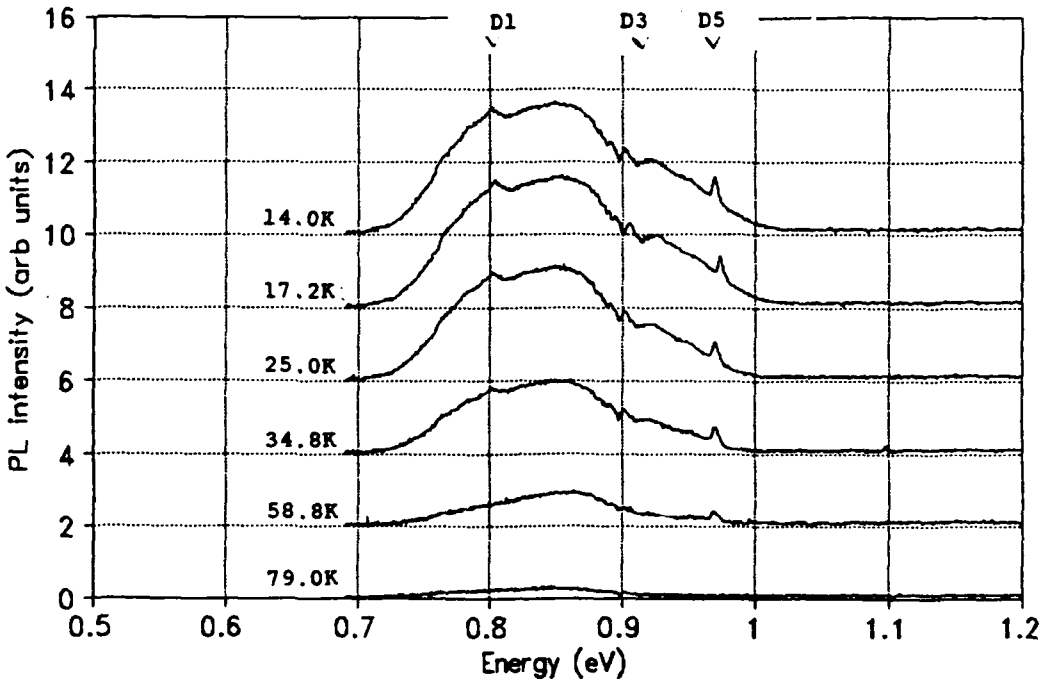


Fig. 19-2. Broad Energy Luminescence Spectra of Sample 201.1 at higher temperature

Table 5 cont'd

| Temp.(K) | Peak Intensity | Peak Position(eV) | Linewidth(eV) | Integrated Intensity |
|---|---|---|---|---|
| 14.0 | 6.95 | 0.85 | 0.17 | 1.1815 |
| 17.2 | 6.89 | 0.85 | 0.176 | 1.2126 |
| 25.0 | 5.92 | 0.85 | 0.168 | 0.9946 |
| 34.8 | 3.77 | 0.848 | 0.162 | 0.6107 |
| 58.8 | 1.65 | 0.858 | 0.15 | 0.2475 |
| 79.0 | 0.42 | 0.845 | 0.127 | 0.0533 |

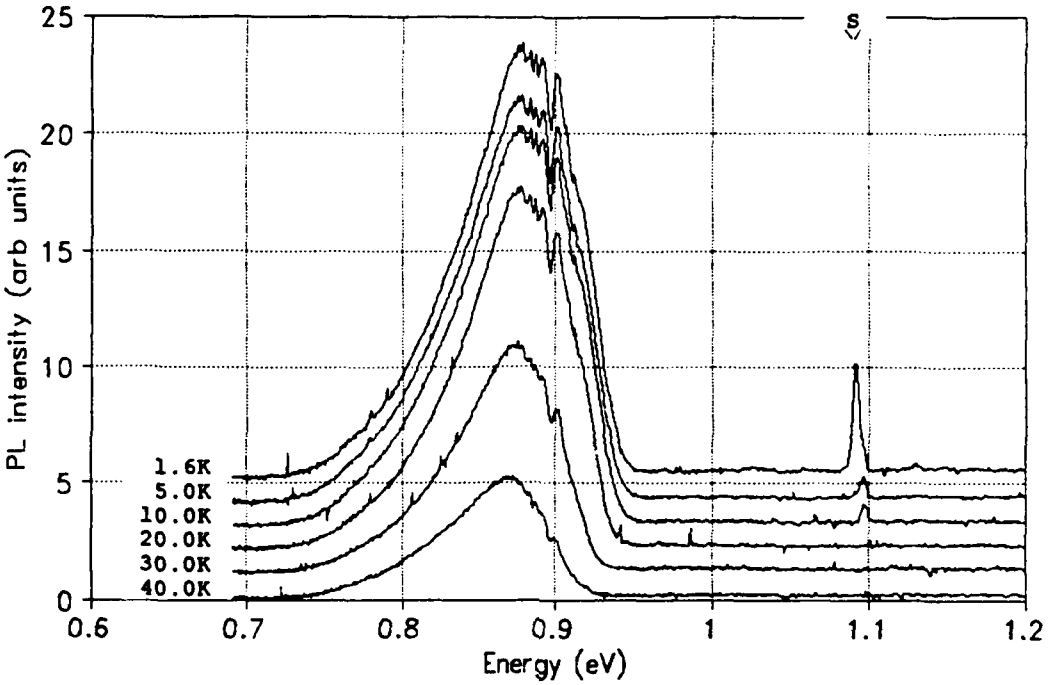


Fig. 20. Broad Energy Luminescence Spectra of Sample 10531.1

Sample ID: 10531.1
Well Width/Barrier Width: 70 angstroms/140 angstroms
Number of Periods: Approx. 25
Nominal Ge Concentration x: 0.24

Table 6
Broad Energy Luminescence Spectra of
$Si_{0.76}Ge_{0.24}$(70 Å)/Si(140 Å) sample

| Temp.(K) | Peak Intensity | Peak Position(eV) | Linewidth(eV) | Integrated Intensity |
|---|---|---|---|---|
| 1.6 | 18.20 | 0.883 | 0.091 | 1.6562 |
| 5.0 | 17.00 | 0.879 | 0.093 | 1.5810 |
| 10.0 | 16.82 | 0.879 | 0.091 | 1.5306 |
| 20.0 | 15.15 | 0.879 | 0.089 | 1.3408 |
| 30.0 | 9.60 | 0.872 | 0.078 | 0.7488 |
| 40.0 | 5.00 | 0.869 | 0.073 | 0.3650 |
| 60.0 | 0.77 | 0.8515 | 0.085 | 0.0655 |
| 80.0 | 0.19 | 0.839 | 0.089 | 0.0169 |

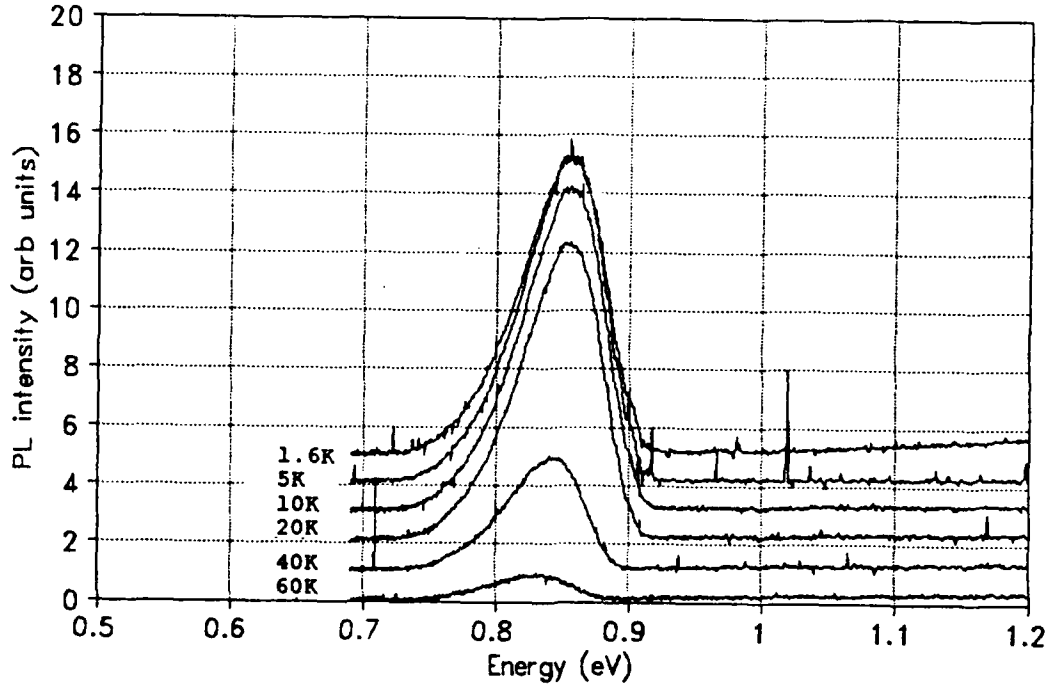


Fig. 21. Broad Energy Luminescence Spectra of Sample 10206.1

Sample ID: 10206.1
Well Width/Barrier Width: 70 angstroms/140 angstroms
Number of Periods: Approx. 25
Nominal Ge Concentration x: 0.3

Table 7
Broad Energy Luminescence Spectra of $Si_{0.70}Ge_{0.30}$(70 Å)/Si(140 Å) sample

| Temp.(K) | Peak Intensity | Peak Position(eV) | Linewidth(eV) | Integrated Intensity |
|---|---|---|---|---|
| 1.6 | 10.03 | 0.855 | 0.072 | 0.7222 |
| 5.0 | 10.97 | 0.855 | 0.072 | 0.7898 |
| 10.0 | 10.87 | 0.854 | 0.072 | 0.7826 |
| 20.0 | 10.02 | 0.852 | 0.070 | 0.7014 |
| 40.0 | 3.73 | 0.842 | 0.068 | 0.2536 |
| 60.0 | 0.785 | 0.832 | 0.067 | 0.0526 |
| 80.0 | 0.14 | 0.829 | 0.059 | 0.0083 |

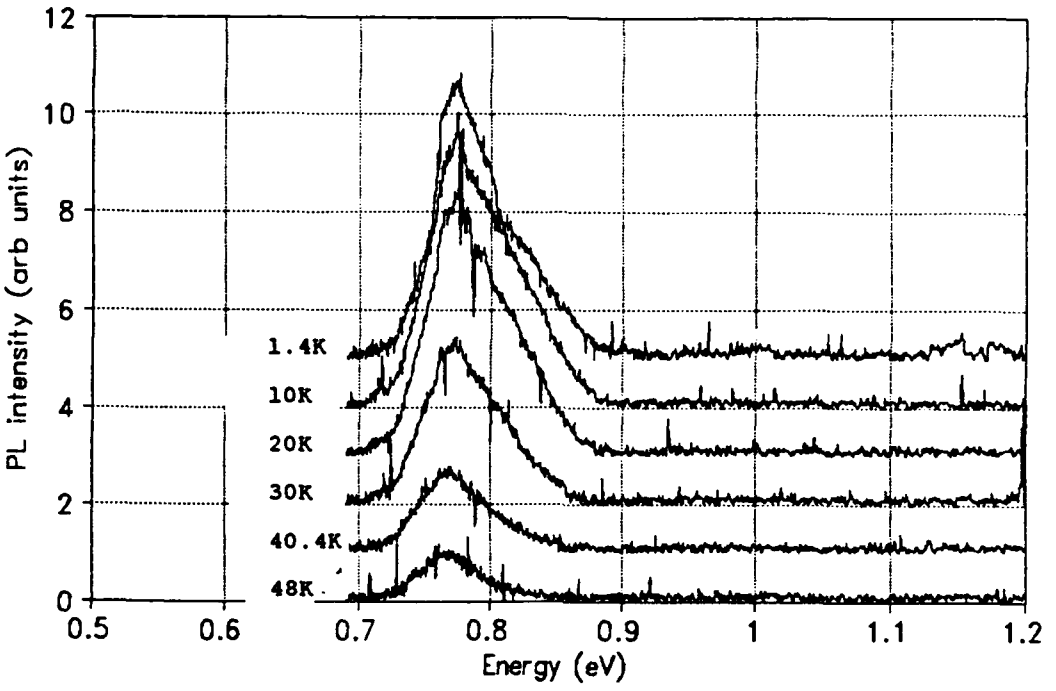


Fig. 22. Broad Energy Luminescence Spectra of Sample 405.1

Sample ID: 405.1
Well Width/Barrier Width: 40 angstroms/80 angstroms
Number of Periods: Approx. 40
Nominal Ge Concentration x: 0.35

Table 8
Broad Energy Luminescence Spectra of
$Si_{0.65}Ge_{0.35}$(40 Å)/Si(80 Å) sample

| Temp.(K) | Peak Intensity | Peak Position(eV) | Linewidth(eV) | Integrated Intensity |
|---|---|---|---|---|
| 1.4 | 5.45 | 0.774 | 0.050 | 0.2725 |
| 10.0 | 5.20 | 0.772 | 0.075 | 0.3900 |
| 20.0 | 5.25 | 0.772 | 0.070 | 0.3675 |
| 30.0 | 3.20 | 0.722 | 0.066 | 0.2112 |
| 40.4 | 1.61 | 0.769 | 0.056 | 0.0902 |
| 48.0 | 0.946 | 0.764 | 0.046 | 0.0435 |

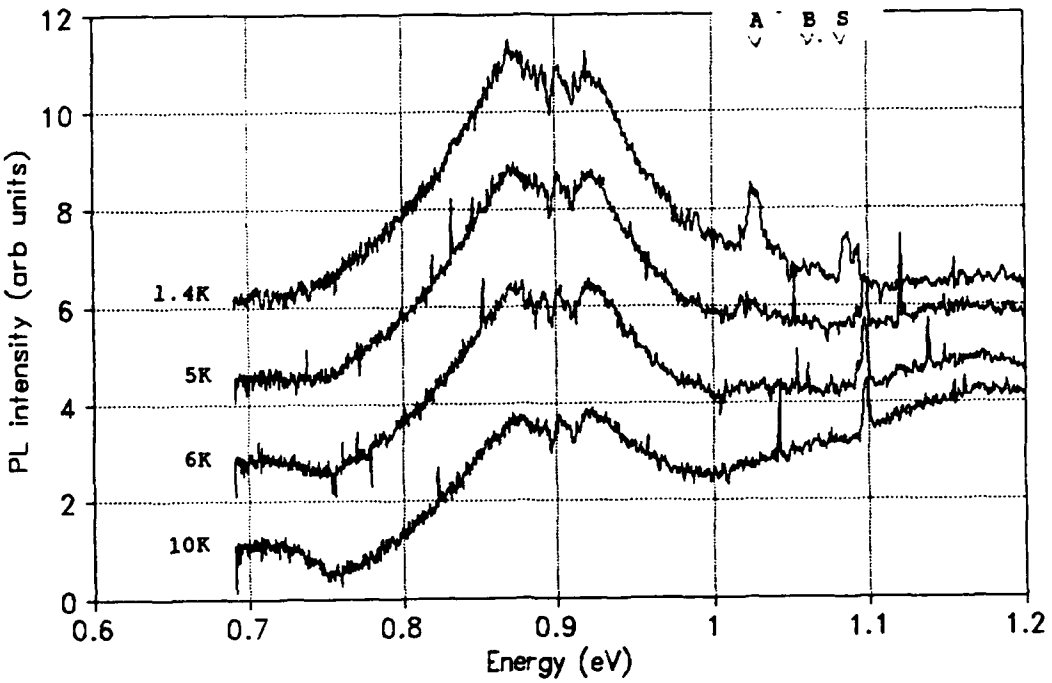


Fig. 23. Broad Energy Luminescence Spectra of Sample 10415.2

Sample ID: 10415.2
Well Width/Barrier Width: 20 angstroms/40 angstroms
Number of Periods: Approx. 80
Nominal Ge Concentration x: 0.25

Table 9
Broad Energy Luminescence Spectra of
$Si_{0.75}Ge_{0.25}$(20 Å)/Si(40 Å) sample

| Temp.(K) | Peak Intensity | Peak Position(eV) | Linewidth(eV) | Integrated Intensity |
|---|---|---|---|---|
| 1.4 | 4.85 | 0.872 | 0.125 | 0.6063 |
| 5.0 | 3.40 | 0.872 | 0.109 | 0.3706 |
| 6.0 | 2.25 | 0.870 | 0.096 | 0.2160 |
| 10.0 | 1.35 | 0.870 | 0.084 | 0.1134 |

Substrate Lines: A = 1.02 eV
B = 1.07 eV

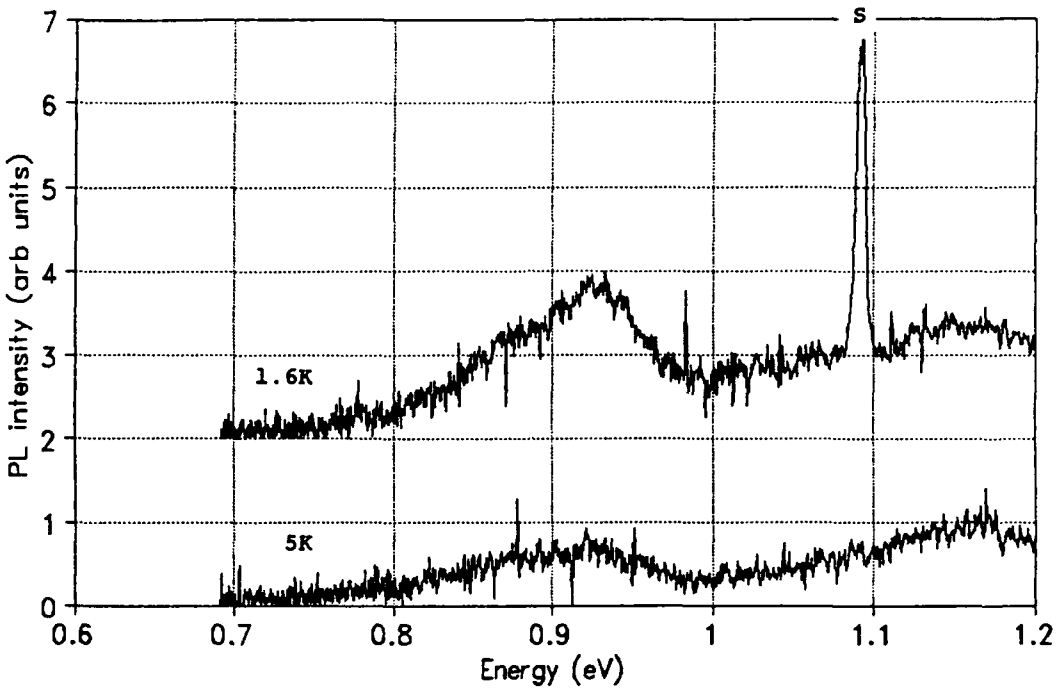


Fig. 24. Broad Energy Luminescence Spectra of Sample 10416.1

Sample ID: 10416.1
Well Width/Barrier Width: 10 angstroms/20 angstroms
Number of Periods: Approx. 160
Nominal Ge Concentration x: 0.25

Table 10
Broad Energy Luminescence Spectra of
$Si_{0.75}Ge_{0.25}$(10 Å)/Si(20 Å) sample

| Temp.(K) | Peak Intensity | Peak Position(eV) | Linewidth(eV) | Integrated Intensity |
|---|---|---|---|---|
| 1.6 | 1.05 | 0.928 | 0.056 | 0.0588 |
| 5.0 | 0.40 | 0.928 | 0.095 | 0.0380 |

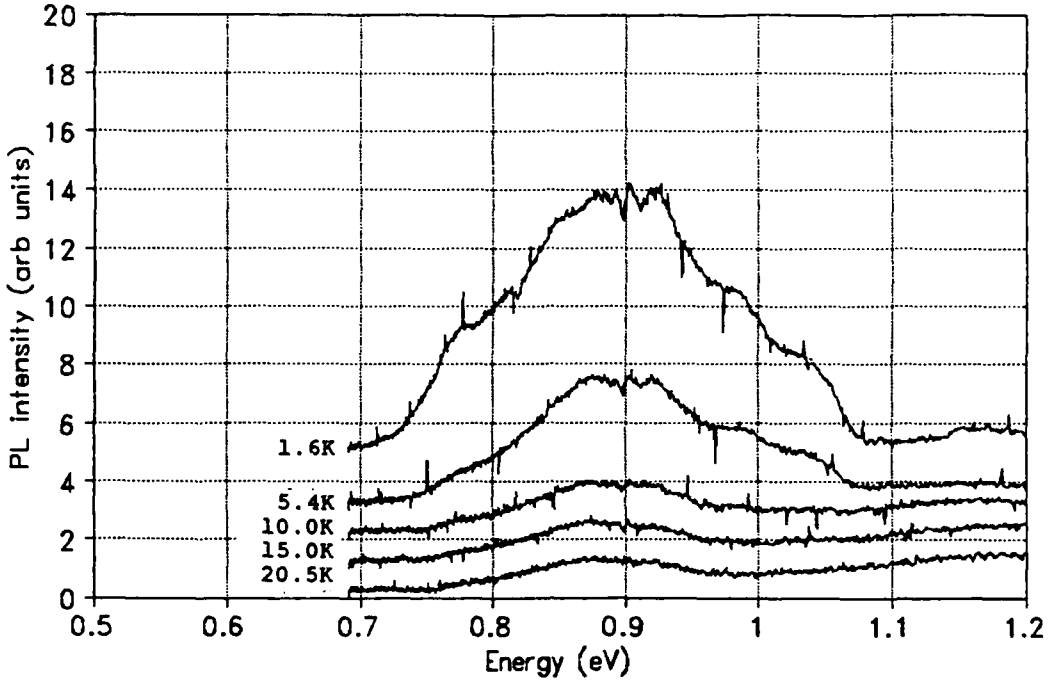


Fig. 25. Broad Energy Luminescence Spectra of Sample 326.1

Sample ID: 326.1
Well Width/Barrier Width: 13 angstroms/26 angstroms
Number of Periods: Approx. 125
Nominal Ge Concentration x: 0.25

Table 11
Broad Energy Luminescence Spectra of
$Si_{0.75}Ge_{0.25}$(13 Å)/Si(26 Å) sample

| Temp.(K) | Peak Intensity | Peak Position(eV) | Linewidth(eV) | Integrated Intensity |
|---|---|---|---|---|
| 1.6 | 9.05 | 0.900 | 0.192 | 0.1738 |
| 5.4 | 3.80 | 0.895 | 0.152 | 0.5776 |
| 10.0 | 1.19 | 0.890 | 0.085 | 0.1012 |
| 15.0 | 0.78 | 0.880 | 0.090 | 0.0702 |
| 20.5 | 0.63 | 0.877 | 0.100 | 0.0630 |

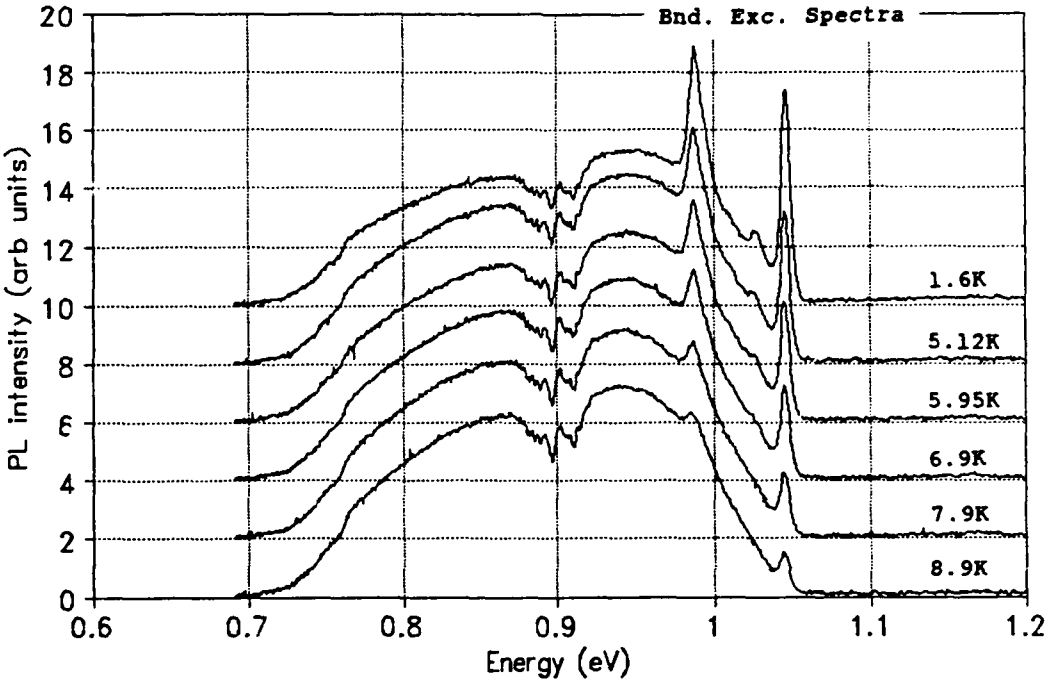


Fig. 26-1. Broad Energy Luminescence Spectra of Sample 206.1 at lower temperature

Sample ID: 206.1
Well Width/Barrier Width: 20 angstroms/40 angstroms
Number of Periods: Approx. 80
Nominal Ge Concentration x: 0.25
Annealing: 575°C, 30 sec (RTA)

Table 12
Broad Energy Luminescence Spectra of
$Si_{0.75}Ge_{0.25}$(20 Å)/Si(40 Å) sample

| Temp.(K) | Peak Intensity | Peak Position(eV) | Linewidth(eV) | Integrated Intensity |
|---|---|---|---|---|
| 1.6 | 5.40 | 0.922 | 0.239 | 1.2906 |
| 5.12 | 6.55 | 0.922 | 0.230 | 1.5065 |
| 5.95 | 6.55 | 0.922 | 0.231 | 1.5131 |
| 6.9 | 7.05 | 0.922 | 0.228 | 1.6074 |
| 7.9 | 7.25 | 0.922 | 0.227 | 1.6458 |
| 8.9 | 7.28 | 0.922 | 0.228 | 1.6598 |

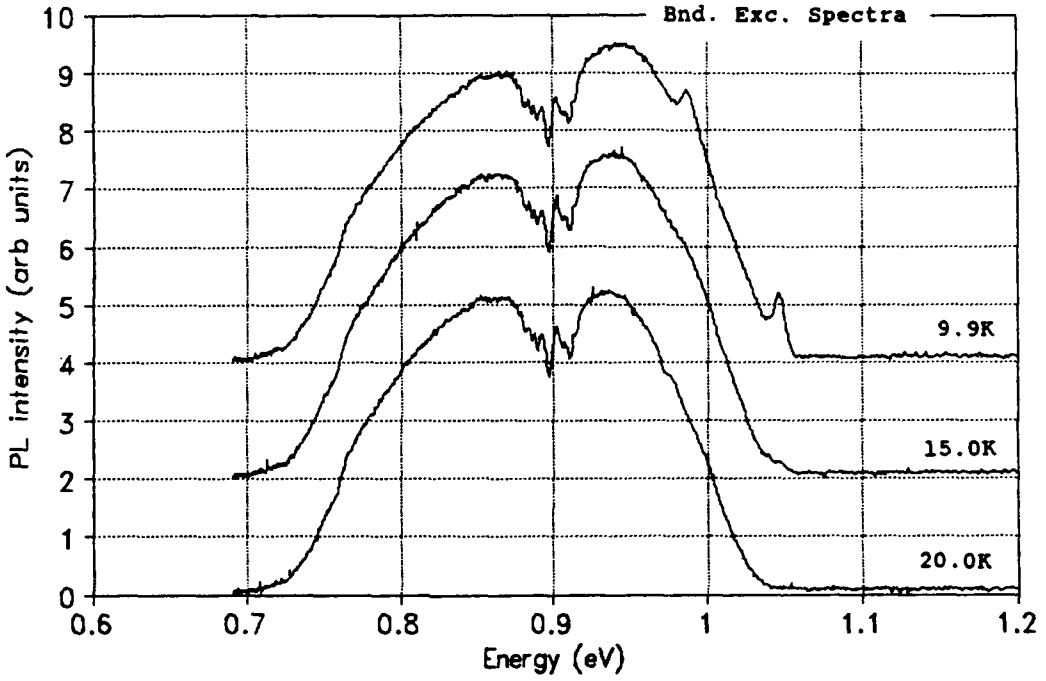


Fig. 26-2. Broad Energy Luminescence Spectra of Sample 206.1 at Intermediate Temperature

Table 12 cont'd

| Temp.(K) | Peak Intensity | Peak Position(eV) | Linewidth(eV) | Integrated Intensity |
|---|---|---|---|---|
| 9.9 | 11.1 | 0.922 | 0.235 | 2.6085 |
| 15.0 | 11.6 | 0.907 | 0.228 | 2.6448 |
| 20.0 | 10.6 | 0.907 | 0.220 | 2.3320 |

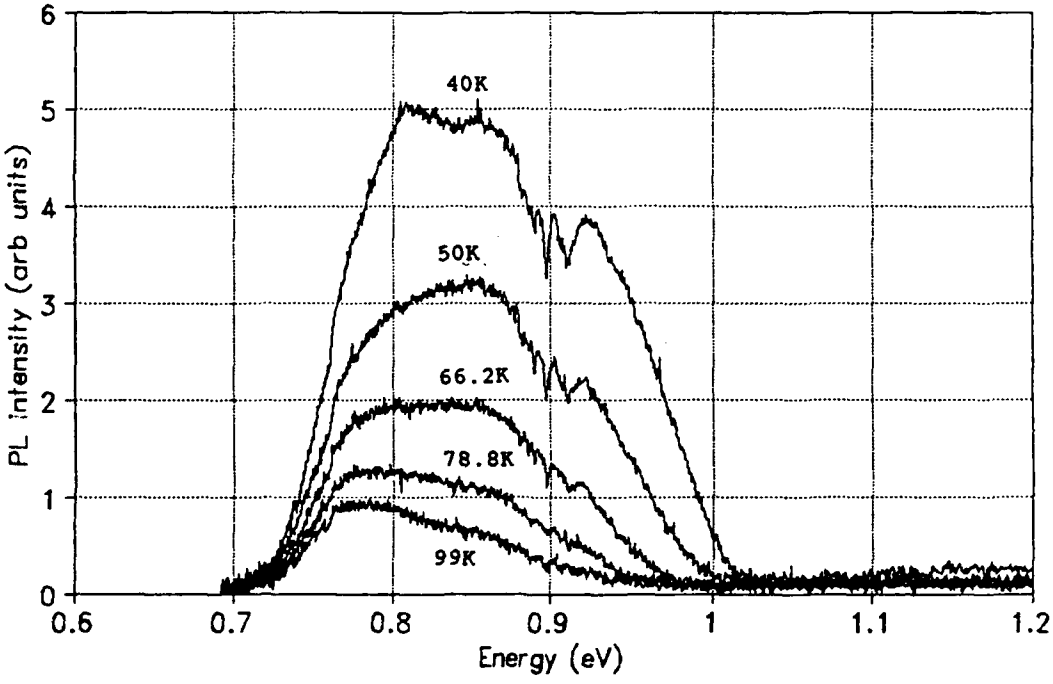


Fig. 26-3. Broad Energy Luminescence Spectra of Sample 206.1 at higher temperature

Table 12 cont'd

| Temp.(K) | Peak Intensity | Peak Position(eV) | Linewidth(eV) | Integrated Intensity |
|---|---|---|---|---|
| 40.0 | 5.8 | 0.848 | 0.188 | 1.0904 |
| 50.0 | 3.2 | 0.848 | 0.184 | 0.5888 |
| 66.2 | 1.93 | 0.848 | 0.173 | 0.3339 |
| 78.8 | 1.28 | 0.79 | 0.134 | 0.1715 |
| 99.0 | 0.92 | 0.79 | 0.155 | 0.1426 |

## VI. Discussion

### Part 1

Part 1 pertains to the sharp peaks in samples 201.1, 206.1, and 1322.2 located at 0.95 to 1.05 eV. These peaks are shown in Fig. 15-17.

Comparison of these spectra with those reported by Sturm et al.[27] suggests the following identifications: the peak labelled "NP" in each spectrum is a no-phonon transition associated with bound exciton recombination in the alloy. The peaks labelled TA, B, C, and D in Fig. 15 and 16 are, respectively, the transverse acoustic (TA) phonon replica, Ge-Ge transverse optic (TO), Si-Ge TO, and Si-Si TO phonon replica.

Identification of the peaks is based on the peaks' position relative to the alloy bandgap and each other. As mentioned in Section II, Eq. (8), the exciton levels in a SL occur above the well bandgap, and, even after subtracting the exciton binding energy, the bound exciton recombination energy may still be above the bandgap. Therefore, the NP peak is identified as recombination of an exciton bound to a shallow impurity in the alloy. The other labelled peaks are identified from their positions relative to the NP. In bulk Si, the energies of the TA and Si-Si TO phonons are well known[28:94]. As shown in the table below, the relative positions of the labelled peaks in Fig. 15-17 match those expected for these phonon energies.

TABLE 13
Proposed Si Peak Assignments

| Sample | Peak | Separation From NP(eV) | Expected Separation (Davies) |
|---|---|---|---|
| 00206.1 | TA | 0.019 | 0.0184 |
| | Si-Si TO | 0.058 | 0.058 |
| 00201.1 | TA | 0.0165 | 0.0184 |
| | Si-Si TO | 0.0575 | 0.058 |
| 00322.2 | TA | 0.018 | 0.0184 |
| | Si-Si TO | 0.058 | 0.058 |

The relative positions of peaks B and C also match those reported by Sturm et al. for the Ge-Ge TO and Si-Ge TO phonon replicas, respectively.

TABLE 14
Proposed Alloy Peak Assignments

| Sample | Peak | Separation From NP(eV) | Expected Separation (Sturm et al.) |
|---|---|---|---|
| 00206.1 | Ge-Ge TO | 0.037 | 0.035 |
| | Si-Ge TO | 0.0512 | 0.0505 |
| 00201.1 | Ge-Ge TO | 0.0345 | 0.035 |
| | Si-Ge TO | 0.0475 | 0.0505 |

In the spectrum of sample 10322.2, the peak labelled X partly obscures the Ge-Ge and Si-Ge TO peaks. The position of X is 0.991 eV, slightly lower than the expected Ge-Ge TO peak (40 meV below the NP). Also, X persists until the temperature is raised to 40 K, indicating a high activation energy. Comparison with the transitions reported by Davies[28:181] and its activation energy suggests X may be a dislocation-related line, D4, in Si[29].

Also in the same spectrum, the peak marked "S" is emission from the substrate. This has been reported in published literature[11;24]. It is believed to be a phonon-assisted bound-exciton transition in the substrate.

The physical meaning of the NP transitions and phonon replicas is as follows[30:5684,5692]. As described in Section II, in pure Si or Ge the energy bandgap is indirect, meaning the conduction and valence band edges are separated in momentum space. Thus a radiative recombination of an impurity-bound exciton requires creation of a phonon to conserve momentum. In an alloy, however, the Si and Ge atoms act as momentum-conserving impurities to each other, and a no-phonon transition is therefore allowed. This transition is more likely to occur with excitons bound to deeper impurities. Thus, with shallow impurities, the NP peaks will be weak. Phonon-assisted transitions, of course will still occur, giving rise to the phonon replicas at lower energies. In a Si-Ge alloy, there are three different TO phonons possible, corresponding to motion of Si-Si, Ge-Ge, and Si-Ge atom pairs. There are also TA and LA phonons. The phonon replicas will be more intense than the NP line; in Si and Si-rich alloys, TO phonon replicas will be strongest, followed by TA replicas.

Binding Energy

The intensity I of the bound-exciton recombination line as a function of temperature T is given by[6:120]:

$$\frac{I(T)}{I(T_0)} = \frac{1}{1 + T^{3/2}\ C\ \exp(-E_a/kT)} \qquad (11)$$

where $E_a$ is the binding energy of the exciton to the impurity. A least-squares fit of Eq. (11) to the data gives the following (approximate) binding energies:

TABLE 15
Exciton Binding Energies

| SAMPLE | BINDING ENERGY (meV) |
|---|---|
| 00206.1 | 4.3 |
| 00201.1 | 4.5 |
| 10322.2 | 5.2 |

These agree fairly well with the binding energies of excitons in bulk Si[28:121] and Si-Ge alloys[30:5686] which are around 5 meV.

In a SL, as mentioned in Section II, the quantum well structure generally leads to an increase in binding energy. This has been observed in GaAs/GaAlAs SLs where exciton recombination lines can be seen even at room temperature[32:223]. The fact that the binding energies in the SL samples in this project are similar to bulk materials seems to suggest they have been reduced in some way. In AlGaAs/GaAs SLs the binding energy of impurities is known to vary significantly as a function of well width. In particular, the binding energy to a donor at the center of a well reaches a sharp maximum of four times the bulk value at a well width of 10 to 40 angstroms, depending on the Al concentration, and decreases rapidly as the well width decreases below or increases above this critical value[33:207]. For relatively wide

wells, the binding energy is the same as for bulk materials. In addition, the binding energy is highest for impurities at the center of the well, and for atoms near the edge can be as much as 5 meV lower[32:221] (see Fig. 27).

The explanation for the well-width/binding energy relationship is as follows[33:207]: for an infinitely wide well,

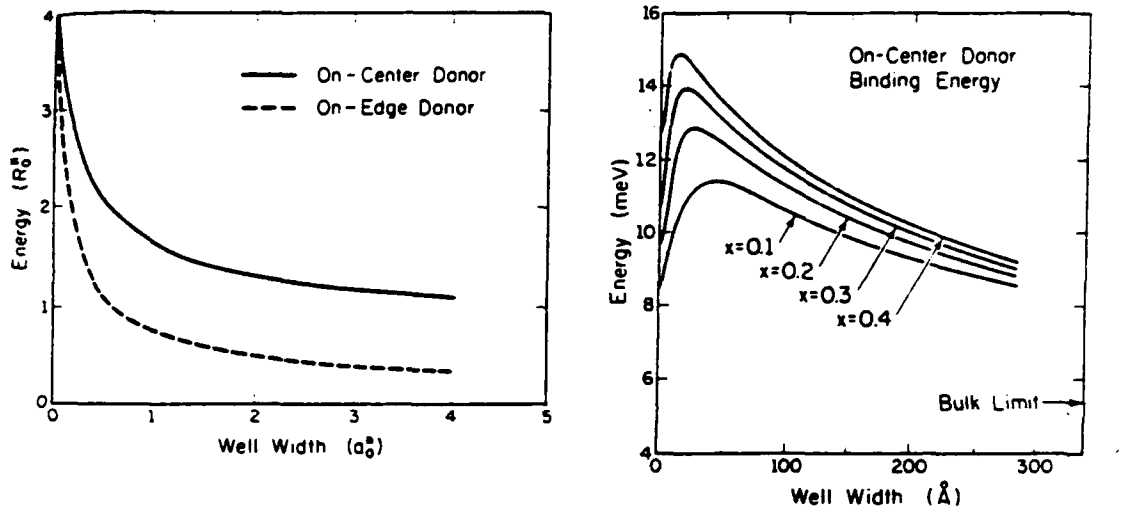


Fig. 27. Exciton Binding Energy as a Function of Well Width for GaAs/$Al_xGa_{1-x}As$ Quantum Wells[33:207]

the binding energy is that of bulk GaAs. As the well becomes narrower, the lowest conduction band rises in energy as an effect of the spatial confinement of the electrons. The impurity binding energy also increases, but not as much as the conduction band because the electron's wavefunction is already limited by the impurity attraction and does not interact with the barriers as much. Thus, as the well narrows there is an increasing difference between the conduction band edge and the impurity level. That is, the impurity binding energy increases. When the

well width reaches zero, only bulk AlGaAs is left, and the binding energy corresponds to that material. Since the binding energy in AlGaAs is less than for a finite-width quantum well, it follows that the binding energy must reach a maximum at some well thickness and then decrease.

We can apply this picture directly to Si-Ge SLs. When the well width reaches zero, the binding energy is that of pure Si. Although Si has a higher binding energy than a Si-Ge alloy, the binding energy of some finite quantum well will be even higher. Thus the binding energy will reach a maximum at some nonzero well width and then drop off to the pure Si value. Then an explanation for the relatively low binding energies observed in this project is that the well widths of the samples studied are wider than the critical value, such that the impurity binding energies are lowered to the bulk alloy values. The samples studied by Sturm et al. have the same well thicknesses, 23 to 34 angstroms, and the binding energies they reported are also around 5 meV It is also possible that the impurity atoms are near the well edges, decreasing the binding energies further. This appears unlikely, however, given the strong intensity of the NP line. The density of states per unit binding energy is highest for atoms at the center and lower for atoms near the edges, and therefore the strongest transitions are those from atoms at the well center. Furthermore, impurities usually concentrate at specific positions in the well only if the wells are intentionally doped. Residual impurities normally are randomly

dispersed throughout the well.

NP Line Position

An obvious discrepancy in the data is the variation in the NP line position between the three samples. Samples 206.1 and 201.1 both have Ge concentration x=0.25 and 20 angstrom wells, but the NP peak position differs between them by more than 25 meV. Sample 1322.2 has x=0.25 and 40 angstrom wells; thus it should have a peak lower in energy than the other two, not intermediate between them. Possible explanations are that: (1) the well widths are different from the nominal values, or (2) the x values are different from the nominal values.

(1) We can estimate the actual well width for each sample from the relation[33:211]: $h\nu = E_g + E_e + E_h - E_i$, where $h\nu$ is the observed transition energy, $E_g$ is the well bandgap, $E_e$ and $E_h$ are the electron and hole subband energies, and $E_i$ is the binding energy to the impurity. From the known strained-alloy bandgap, the transition energy, and the measured binding energies, we can estimate the electron and hole energy levels. Finally, we assume these levels to be the bound levels for finite square wells. Although this is a relatively standard technique[32:219], this assumption is strictly only valid for wide barriers; specifically barrier widths much greater than the penetration depth of the confined wave function[34:9]. The table below shows the well width that would be required to produce a bound-exciton peak at the observed position.

TABLE 16
Required Well Widths

| Sample | Nominal Well Width(angstroms) | Required Well Width(angstroms) |
|---|---|---|
| 00201.1 | 20 | 19 |
| 00206.1 | 20 | 17 |
| 10322.2 | 40 | 18 |

(2) Likewise we can estimate the actual Ge concentration x of each sample required to produce the observed line positions.

TABLE 17
Required Ge Concentrations

| Sample | Nominal Ge Concentration | Required Ge Concentration |
|---|---|---|
| 00201.1 | 0.25 | 0.25 |
| 00206.1 | 0.25 | 0.24 |
| 10322.2 | 0.25 | 0.20 |

The required change in well width is significant, especially for sample 1322.2. Therefore, it seems more likely that the line position discrepancy is caused by the Ge concentration being different from its nominal value.

Linewidth

The NP linewidth of each sample at 1.6 K, after correcting for the spectrometer resolution, is about 4 to 6 meV. This is about 10 times wider than in bulk Si[35:5358]. Here are two possible explanations:

(1) Effect of the alloy[36:814]. It is known that both elemental and binary III-V compounds such as GaAs produce sharp, narrow bound-exciton recombination peaks. However, in ternary compounds such as $Al_xGa_{1-x}As$, line broadening occurs from the statistical distribution of atoms. If $V_{exc}$ is the volume enclosed by one exciton radius and N is the average number of lattice sites, the standard deviation of the alloy composition is given by the binomial distribution

$$S_x = ( x(1-x) / NV_{exc} )^{1/2} \qquad (12)$$

and then the standard distribution of the bandgap $E_g$ is

$$S_E = (dE_g / dx) S_x$$
$$= (dE_g / dx) ( x(1-x) / (NV_{exc} )^{1/2} \qquad (13)$$

For $0.01 \leq x \leq 0.45$, the binomial distribution can be approximated by a Gaussian distribution. The full width at half maximum of a Gaussian distribution is 2.36 times the standard distribution. Thus, the bound-exciton linewidth will be

$$dE = 2.36S_E$$
$$= 2.36 (dE_g / dx) ( x(1-x) / (NV_{exc} )^{1/2} \qquad (14)$$

Weber and Alonso[30:5689] derived experimentally the following expression for an $Si_{1-x}Ge_x$ alloy for $0 \leq x < 0.85$:

$$E_g (x) = 1.155 - 0.43x + 0.206x^2 \text{ eV} \qquad (15)$$

from which we obtain, for $x = 0.25$, $dE_g/dx = 0.33$ eV. Along with this value, we take $N = 6 \times 10^{21}$ / cm$^3$ and $V = (4/3)\pi r_{exc}^3$, where $r_{exc}$ is the exciton Bohr radius[30:5691]. To find $r_{exc}$, we assume

the exciton radius varies linearly between the pure Si value of 38 angstroms and the pure Ge value of 110 angstroms. For x=0.25, this gives $r_{exc}$ = 56 angstroms. Substituting these values into eqn. (13) gives dE = 5.07 meV, very close to the observed linewidths.

(2) Effect of well structure fluctuations. Bajaj, Reynolds et al.[32:217-8] describe line broadening in GaAs/GaAlAs quantum wells, and their argument is equally applicable to Si-Ge SLs. The well interfaces are laid down layer-by-layer during MBE growth and as a result will contain clusters of Si and of Si-Ge alloy. If the size of these clusters is much less than the exciton radius, the exciton will not be able to "see" them and the recombination line will be narrow. But if the average cluster size is comparable to the exciton radius, the exciton will be affected and the peak will be wide. The effect of these larger clusters is to change the effective well width, which shifts the transition energy. If $x_i$ is the extra Ge concentration at the interface, then the effective well size will be $W(x_i) = W_0 - (x_i/x)\ M$, where $W_0$ is the nominal well width and M is a monolayer distance (about 2.7 angstroms for an Si-rich alloy). The total transition line will thus consist of a group of peaks, corresponding to different effective well sizes. According to Bajaj, Reynolds et al., $x_i$ can vary from 0 to x over the interface. Thus in general the effective well width can vary from $W_0$ to $W_0$ - M. Using the square-well, semi-infinite barriers assumption, we find that, for a 20 angstrom wide well, a change

in effective width of one monolayer will change the transition energy by about 16 meV. Thus, fluctuations of half a monolayer or less, which have been observed in GaAs quantum wells also[32:222], can easily produce the observed linewidths. In particular, to produce a linewidth of 4 meV requires an x fluctuation of only 0.04, or 19 percent (for x=0.25). Although seemingly rather large, this is not at all unreasonable over very small areas of the interface.

Temperature Shift

Finally, we discuss one additional feature of the NP peak, the shift to lower energy as the temperature is raised. The shift is by about 2 meV for each sample. Mitchard and McGill provide an explanation[35:5358-9]. The binding energy of excitons located at different points in the alloy will differ slightly. This is because the impurity binding energy depends on the local concentration of Si and Ge atoms: the more Si, the higher the binding energy. The bound-exciton peak is therefore actually composed of a group of closely spaced lines, each corresponding to a different local distribution of atoms. At low temperature, all lines contribute to the peak. As the temperature is raised, however, the more loosely bound excitons are ionized, and the peak will come from the tightly bound ones. Because of their higher binding energy, these have a lower recombination energy, and thus the total peak shifts to lower energy.

An alternative explanation is based on the analysis of

Bajaj, Reynolds et al. presented earlier. Local fluctuations in the Ge concentration at the well interfaces can change the effective well size by as much as a monolayer. As mentioned above, for the well widths used in this project such a change or less can easily produce the observed peak shift. At low temperatures the emission is from all wells. As the temperature is raised, the wider effective wells with their higher energy bound states constitute most of the emission, since the narrower wells have been ionized.

Part 2

Next we turn to the broad luminescence band (which we will call the broad energy luminescence or BEL). Fig. 18-26 show the BEL for various samples. As mentioned in Section III, a similar peak has been observed for both alloy and alternating Si-Ge layer SLs and attributed to different phenomena. However, the cause of the peak is unknown for certain.

The major features of the BEL spectra are:

(1) Large integrated intensity. The peak is both high and wide. At its height it is about twice as high as the NP line described in Part 1. For example, in sample 10322.2 the peak at 4.4 K is 4.55, twice as high as the NP line at the same temperature. In sample 206.1 the BEL peak reaches a maximum height of 11.2, nearly twice as high as the maximum of the NP line, which starts

at 6.45 and then decreases. ALso, the maximum linewidth of the BEL peak in 10322.2 is 167 meV, 19 times that of the NP line. The combination of height and linewidth leads to an integrated intensity 25 times that of the NP line.

(2) Narrowing linewidth as temperature rises. Again referring to spectra of sample 10322.2 shown in Fig. 18 and the accompanying table, we see the linewidth monotonically decreasing as the sample temperature is raised. Not all samples show such a steady decline; for instance see sample 326.1 in Fig. 25. But in all samples the trend is toward lower linewidth at higher temperature. In addition, looking at the BEL spectra, especially Fig. 26, the peak loses width from its high-energy side, becoming more asymmetric, at higher temperatures.

(3) Peak location at about 50-100 meV below bandgap. For each sample, the BEL peak at 1.5 K is between 50 and 100 meV below the bandgap. This feature is discussed further below.

(4) Peak height increases up to about 10-15 K, then decreases. This feature is illustrated by samples 201.1, Fig. 19, and 206.1, Fig. 26. Note that in sample 206.1 the initial rise in the BEL peak height is coincident with the decline in the NP line intensity. But not all samples showed this initial rise: in sample 10531.1, Fig. 20, the BEL peak continually decreases in intensity as temperature rises.

(5) Peak shift to lower energy at higher temperature. For each sample the peak shows a shift to lower energy as the temperature is increased from 1.5 to 80 K. The greatest shift is in sample

206.1, in which the peak shifts from 0.922 to 0.79 eV. In other samples, such as 201.1, the shift is hardly noticeable.

The temperature dependence curve of the BEL peak is characteristic of the thermal activation of bound excitons from a lower to higher bound state or from bound to free. This activation is described by the expression[29:9]

$$I(T)/I(0) = 1 / [1 + C \exp(-E/kT)] \qquad (16)$$

where I is the intensity at temperature T, E is the activation energy, and C is a constant which incorporates the degeneracy and radiative lifetimes of the involved states. A least-squares fit of eqn. (16) to the data gives the activation energies listed below (at least 5 data points were required before a fit was attempted):

TABLE 18
Activation Energies

| Sample | Activation Energy(meV) |
|---|---|
| 10206.1 | 38.10 |
| 10531.1 | 27.74 |
| 201.1 | 30.39 |

Now we list several possible causes of the BEL in these samples. In each section we assume the peak is caused by that particular mechanism and list the expected peak energy position and effect on the peak of changes in temperature, Ge concentration, and SL well width.

(1) Isoelectronic traps in Si.

Energy position: approx. 50-150 meV below bandgap

Temperature dependence: No-phonon lines at low temperature; phonon broadened luminescence at higher temperature

Ge concentration dependence: higher energy for lower x

Well width dependence: higher energy for narrower wells

It has been known since 1962 that excitons can become bound to isoelectronic traps in semiconductors and emit characteristic recombination radiation[42:2401]. An atom or group of atoms of the same total valence as the host material occupies a lattice site, creating a short-range potential. This local potential first tightly binds one carrier, most commonly an electron, whereupon it becomes charged. The charged trap then loosely binds a hole by its Coulomb field, thereby creating a bound exciton.

The most likely candidate for an isoelectronic trap in the samples studied is Ge; that is, the Ge atoms in the Si-rich alloy act as isoelectronic centers for the Si. Although no published data are readily available on Ge traps in Si, a number of other isoelectronic impurities have been extensively studied in Si[37-43] and comparison will be made of the BEL luminescence with this data.

The x- and well width-dependences match that of the BEL peak. However, the spectral features are significantly different:

1. PL spectra from isoelectronic traps in Si include sharp,

no-phonon spikes. The linewidth is 0.5 meV or lower, much less than the BEL peak. Also, the NP spikes are at 1.1 to 1.16 eV. Most of the samples studied here do not show any structure in this range. The BEL luminescence is at 0.77 to 0.92 eV. Finally, the spikes broaden at higher temperature, whereas the BEL peak narrows.

2. Some spectra, such as Se-doped Si[38], do show a broad, phonon band displaced at higher energy than the NP lines. The phonon band is at 0.95 eV and its shape is similar to the BEL luminescence. However, unlike the BEL peak, the phonon band is very low in intensity below 45 K increases in intensity and linewidth between 45 K and 75 K. In fact, its highest integrated intensity is around 75 K, where the BEL peak has almost vanished. Second, at temperatures below 45 K the dominant luminescence consists of a sharp transition accompanied by phonon sidebands, all around 0.78 eV. No such peaks are observed for the samples studied here. Finally, the thermal dissociation energy of the phonon band, for Se-Si, is more than 110 meV, much greater than the activation energy of the BEL peak.

Because the energy, spectral and thermal characteristics of the BEL peak are very different from those of isoelectronic centers in Si, we rule out these centers as a likely source of the peak.

(2) Isoelectronic centers combined with alloy broadening.

Energy position: 1.08 to 0.95 eV depending on Ge

concentration

Temperature dependence: No phonon lines at low temperature; larger phonon bands at higher temperature

Ge concentration dependence: Higher energy for lower x

Well width dependence: Higher energy with narrower wells

This possibility involves a third isoelectronic impurity in the Si-Ge alloy creating the BEL peak. Alternatively, the Ge atoms may be responsible, as in (1) above, but the proximity of other Ge atoms nearby may cause additional broadening of the emission. Modavis et al.[44] studied alloys doped with Be for x up to 0.2. The spectra consist of a narrow, no-phonon line at 1.07 eV and a TO phonon replica at 1.02 eV. The no-phonon line is similar to Be-doped Si, but is broadened by alloy effects. This also appears an unlikely source of the BEL luminescence for these reasons:

1. As in (1) above, the BEL luminescence consists of only a broad band. The sharp, no-phonon spikes, which are characteristic of isoelectronic centers even in an alloy, are absent.

2. The BEL peak is much too wide to be a no-phonon line. Modavis et al. found the NP transition linewidth at 10 K to be 10 to 40 meV for x from 0.02 to 0.13. Roughly extrapolating from their curve, the linewidth at x=0.2 is about 43 meV, and at 0.25, 48 meV. This is one-half to one-fourth as wide as the BEL peak. For example, in sample 10322.2, with x=0.2, the BEL linewidth at 9.2 K is 150 meV. Likewise, in sample 10531.1 with x=0.24 the

linewidth is 93 meV. Also, for a given temperature the no-phonon linewidth consistently increases with Ge fraction x, whereas the BEL does not show such behavior.

3. The BEL peak is in the wrong location to be the phonon replica. The phonon band is 150 meV below the alloy bandgap. On the other hand, the BEL peak appears 50 to 100 meV below the strained-alloy gap.

(3) Dislocation-Related Luminescence.

Energy position: Six sharp peaks at fixed locations from 0.812 to 1.013 eV.

Temperature dependence: Broadening and lower intensity at higher temperature

Ge concentration dependence: Broadening at higher x by alloy effects

Well width dependence: None expected

Six dislocation peaks, labelled D1-D6, have been identified in Si[29]. These do not involve impurities; rather, the dislocations themselves are the active recombination centers. They do not change position significantly in Si-rich alloys[44:955]. The peaks are superposed on a broad, low-intensity background.

Dislocations also seem unlikely to be the cause of the BEL peak because:

1. The spectral features are very different. Dislocation-related transitions are characterized by high, sharp spikes at

specific energies. In contrast, the BEL peak is broad, forming a single, relatively smooth peak. MBE grown Si deposited on sputter-cleaned substrates can show a broad band at 0.806 eV, but this is low in intensity and accompanied by much higher D5 and D6 lines located at 1.007 and 0.945 eV.

2. Dislocations cannot account for the BEL peak's rise in intensity at low temperature. The D lines are all constant in intensity up to 10-20 K and then decrease. They also cannot explain the BEL's energy shift; dislocation transitions occur at fxed locations.

3. The activation energies of dislocation lines are 1-10 meV, much lower than that of the BEL peak.

(4) Impurity-bound excitons.

Energy position: 5-10 meV below bandgap

Temperature dependence: thermal broadening at higher temperatures

Ge concentration dependence: Higher energy for lower x

Well width dependence: Higher energy for narrower wells

The Ge and well width dependence match that of the BEL peak. However:

1. The energy position does not fit the location of the BEL peak. The most common impurities in Si all have binding energies close to 5 or 10 meV[8:121]. This matches the location of the NP line described in Part 1.

2. The BEL linewidth is at least 30 times that of the NP

line. The BEL integrated intensity is 60 times greater than that of the NP line. It seems unlikely that impurities would be present in all the samples in such high quantities to produce such an intense peak.

3. Impurity transitions cannot account for the BEL peak's narrowing at higher temperatures, or its losing width on the high energy side.

(5) Electron-Hole Droplets.

Because electrons and holes have anti-parallel spins, the excitons they form are zero-spin particles like bosons. Therefore, it is possible for them to condense into a liquid at low temperatures through Bose condensation[5:452]. This phenomenon has been shown to exist in Si-Ge alloys for Si concentration x=0.15[45]. The luminescence consists of four broad bands at 0.94 to 0.99 eV, and their shape resembles that of the BEL peak. However, the condensed phase exists only near liquid He temperatures and vanishes at about 15 K, leaving the electrons and holes to form a free-exciton gas. In addition, the binding energy per exciton is around 2 meV, much below the BEL activation energy. Moreover, electron-hole droplets are normally formed at high excitation powers, e.g. 3 $W/mm^2$ [8:96], much greater than those used in this project.

(6) Strain-Localized Excitons.

Charge carriers can be confined by strain regions in

crystalline solids. For example, stress applied to a crystal can create a maximum uniaxial strain below the surface, which lowers the bandgap energy. Photoexcited carriers will then be attracted to and confined in the region of maximum strain, known as a strain well. The behavior of strain-confined carriers has been studied in semiconductors[46,47]. In particular, high carrier densities are produced, leading at low temperatures to the electron-hole condensation described above. The shape of the intensity vs photon energy curve is qualitatively similar to the BEL peak near liquid He temperatures: a Maxwell-Boltzmann curve with a slight low-energy tail. However, as in (5) above, the strain luminescence only occurs for very low temperature. It drops exponentially in intensity above 5 K and vanishes above 15 K. The binding energy is 10 meV or less, much lower than the BEL activation energy. The binding energy is mostly independent of the applied stress[46:322]: even stresses up to 100 newtons/mm$^2$ produced no change in the ionization energy. In addition, the strain-confined luminescence shows a threefold increase in linewidth at about 4 K, corresponding to the liquid-gas phase change, which does not occur for the BEL peak.

(7) Quasidirect Bandgap Transition. As mentioned in section III, a peak similar to the BEL has been observed in Si-Ge SLs and attributed to the theoretically-predicted quasidirect bandgap. However, the zone-folding that makes this possible occurs only in short-period SLs. All of the samples studied had long periods of 30 angstroms or more.

Since the above transitions are considered unlikely sources of the BEL peak, an alternative possible cause must be proposed. Alferov et al.[48] showed that local variations in the alloy concentration create potential gradients in the band edges. These in turn exert a force on the charge carriers. For example, in Si-Ge alloys, the conduction band edge is lower, and the valence band edge higher, in regions where the Ge concentration is higher. Thus, potential wells (or hills) are created in the conduction band (or valence band) and the respective charge carriers are attracted to and confined within these traps.

The position of the energy band is[49:1328] $E = E(x) + (dE/dx)\,\delta x$ , where x is the nominal Ge concentration, $E(x)$ is the energy band position corresponding to x, and $\delta x$ is the local variation in x. In a volume $R^3$ of the alloy lattice, there are, on the average, $xNR^3$ Ge atoms where N is the number of lattice sites per unit volume. There are also $(xNR^3)^{1/2}$ excess Ge atoms, assuming large N and a random distribution of atoms[50:16]. This gives

$$\delta x = (xNR^3)^{1/2} / NR^3. \qquad (16)$$

Thus, the depth of the potential well created by this fluctuation is

$$V = (dE/dx)\,(xNR^3)^{1/2} / NR^3. \qquad (17)$$

Just as with any quantum well, the narrower the well is, the higher the confined energy levels. On the other hand, from eqn. (17) we see that the depth V increases with smaller R. The deeper wells will in general have greater band curvature and thus

be more effective at trapping carriers. The most effective wells then are those with the smallest R that contain an energy level. A well will not contain levels if $V < \hbar^2 / M^* R^2$ where $M^*$ is the electron effective mass[49:1328]. Thus, the smallest R is defined by $V = \hbar^2 / M^* R^2$ . Rearranging, we find the depth of these most effective wells to be

$$Vmin = (dE/dx)^4 \, x^2 \, M^{*3} / \hbar^6 \, N^2 \, . \qquad (18)$$

Taking x=0.3, and $N=6 \times 10^{21}/cm^3$ as in Part 1, substitution into eqn. (18) gives Vmin = 48.24 meV. If we approximate the potential well as a finite-barrier square well of depth Vmin, this gives a confined level close to 30 meV, which is the BEL peak activation energy. Substitution into eqn. (17) gives R = 13.71 angstroms, and then into eqn. (16) gives $\delta x = 0.09$. This is about twice as high as the x fluctuation over the well interface found in Part 1.

Although seemingly high, this fluctuation explains the BEL peak shift at high temperatures. The peak shift is caused by progressive thermal ionization of potential wells[30:5687], a similar effect to that proposed in Part 1. At low temperatures, all of the band edge wells participate in the recombination luminescence. At higher temperatures, however, the more shallow wells are ionized, and only the deeper wells radiate. Because these wells are deeper, the band edges are closer together, and thus the photon energy emitted is lower.

Let us take some specific examples. Consider, for instance, sample 10206.1, with x=0.3. For this sample, R = 13.71 angstroms

and $\delta x$ = 0.09. Thus, the shallower wells have x=0.30, V = 48 meV, and the deeper wells have x=0.39, which means V = 81.53 meV, or about 33 meV deeper. The actual peak shift for this sample was 26 meV, fairly close. Likewise, for sample 10531.1, x=0.24, the shallower wells have depth V = 33 meV and again $\delta x$ = 0.09. Thus, the deeper wells have x=0.33 and V = 58 meV, or 27 meV deeper. The actual peak shift was 44 meV, again roughly the same. Finally, consider sample 326.1. For this sample, x=0.25, V = 35.85 meV and still $\delta x$ = 0.09. The shallower wells have x=0.25 and V = 36 meV, the deeper wells have x=0.34 and V = 62.61 meV, or 28 meV deeper. The actual peak shift, between 1.6 K and 20.5 K, was 23 meV.

The potential well picture also possibly explains three other features of the BEL luminescence. First, the linewidth narrowing at high temperature is caused, like the peak shift, by progressive ionization of shallower wells. As the temperature is raised, the higher-energy wells are ionized, and the BEL peak loses width mainly from its high-energy side and becomes less symmetric. For instance, see sample 10531.1, Fig. 20. Second, the initial increase in intensity below 15-20 K occurs because over this temperature range, excitons become dissociated from impurities and more of them become trapped in the fluctuation wells. At liquid He temperatures, the excitons are attracted to shallow impurities, which are closer in energy to the band edges and thus have a higher transition probability. In samples 201.1, 206.1, and 10322.2 these bound excitons recombine radiatively; in

the other samples they may recombine nonradiatively. The reason for this is unknown. As the temperature is raised, these bound excitons are detached from the impurities and free to move through the crystal, where many become attracted to the potential wells and recombine inside the wells, thus increasing the BEL intensity. Finally, the low-energy tail present in some samples, such as 10322.2 and 10206.1, is caused by deep wells. No high-energy tail is observed because the very shallow wells either contain no bound levels, or are quickly ionized at very low temperatures.

Several sample spectra exhibit unusual features. In 326.1, Fig. 25, besides the main peak at 0.9 eV, four other peaks seem to be present, two on either side. The side peaks are mostly gone at 10 K, and the main peak vanishes above 20 K. Sample 405.1, Fig. 22, shows a "knee" on the high energy side at 1.4 K, which is gone by 10 K. Samples 10322.2 and 206.1, Fig. 18 and 26, show a drop in intensity on the low-energy side of the peak as the temperature is raised to 10 K. The latter may be related to a phonon replica. Lai and Klein[51] reported a peak in indirect-bandgap GaAsP which they attributed to excitons bound to alloy fluctuations; this peak also showed several phonon sidebands, lower in energy than the main peak, which decreased in intensity with temperature at the same rate as the main peak.

In some samples, such as 326.1 (Fig. 25), 10416.1 (Fig. 24), and 10415.1 (Fig. 23), the BEL peak declined in intensity quickly with temperature and vanished at a relatively low temperature.

This may be due to the size of the alloy: 326.1 and 10416.1 had thin alloy layers (13 and 10 angstroms respectively), thus no chance to form significant numbers of potential wells. However, 10415.1 had relatively wide alloy layers, but the BEL intensity still dropped quickly. The intensity probably depends on the quality of the alloy: more homogeneous alloys will have fewer potential wells, and the bound states formed in those wells will ionize very rapidly; thus the BEL intensity will be lower. Weber and Alonso[30:5687] found reported a peak similar to the BEL in bulk alloys, and found the peak shift with temperature depended only on the quality of the sample.

Sample 206.1 (Fig. 26) shows a total peak shift of 132 meV, much larger than that predicted from the potential well model. Three of the peak locations, at 0.922 eV, 0.848 eV, and 0.79 eV, are close to dislocation bands D3, D2, and D1 in Si. In fact, each of those three peak locations is about 25 meV below the nearest dislocation band. In a review article of optical transitions of alloys, Pikhtin[55:257] states that composition fluctuations may alter the properties of impurities and defects in the alloy. In particular, deep centers, with their small Bohr radii, will be considerably affected by alloy fluctuations. It is possible in this case that alloy fluctuations are altering the local potential around the dislocations, in particular altering their activation energies, so that the peak luminescence sequentially shifts to the lower-energy dislocations as the temperature is raised. Weber and Alonso also reported a large

peak shift (about 45 meV) in a sample with intense dislocation related luminescence[30:5687].

Bandgap relationship

Fig. 28 shows the position of the BEL peak for the various samples studied. The bandgap energy is the strained alloy bandgap at 90 K taken from data reported by Lang et al.[52]. The Ge concentrations for samples 10322.2, 201.1, and 206.1 are those found in Part 1. The others are the nominal values.

There is no consistent pattern between the peak position and

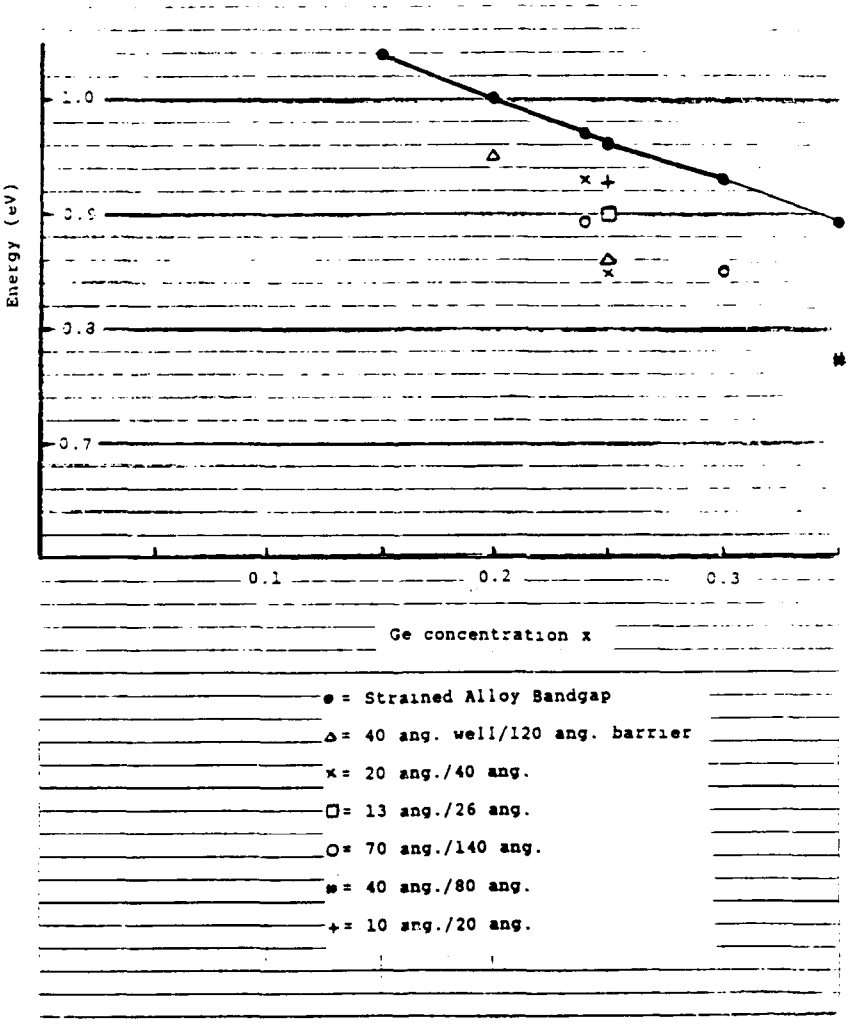


Fig. 28. BEL Relation to Alloy Bandgap.

well width. For x=0.24 and 0.25, the peak is higher in energy for narrower wells; however, comparing the samples at x=0.3 and x=0.35, the x=0.35 sample has a peak farther below the bandgap, even though its wells are narrower. The peak position is found from the relation, given in Part 1, $h\nu = E_g + E_{exc} - E_b$, where $h\nu$ is the observed transition energy, $E_g$ is the well bandgap, $E_{exc} = E_e + E_h$ is the sum of the electron and hole subband energies, and $E_b$ is the exciton binding energy in the well. For narrower wells, $E_{exc}$ and $E_b$ both increase, so the peak position may shift up or down in energy depending on which increases faster.

The BEL peak is about 50 to 120 meV below the bandgap. This implies the binding energy is 20 to 90 meV higher than the activation energy. In their study of a peak similar to the BEL in GaAsP, Lai and Klein[53:3220] found the activation energy of that peak was about 8 meV below the binding energy. They proposed the presence of nearby, higher energy states to which the electron excites and from which it departs nonradiatively. They also suggested that the decrease in the peak width on its high-energy side is partly determined by the amount of coupling to these higher energy states. The greater the coupling strength, the more the high-energy dropoff.

Excitation Power Dependence

Fig. 29-31 show spectra recorded for three samples at different laser powers. The laser was an A ion emitting at 488 +/- 3 nm.

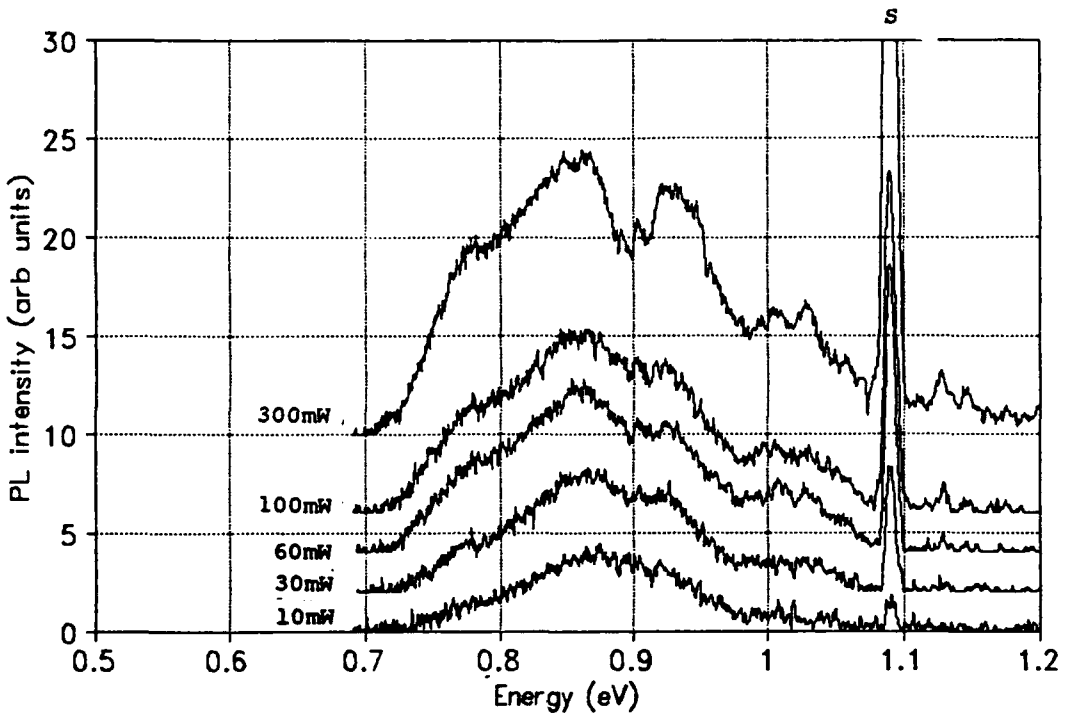


Fig. 29. Broad Energy Luminescence Spectra of Sample 326.1

Sample ID: 326.1
Well Width/Barrier Width: 13 angstroms/26 angstroms
Number of Periods: Approx. 125
Nominal Ge Concentration x: 0.25

Table 19
Sample 326.1 BEL Luminescence

| Exc Pwr(mW) | Peak Intensity | Peak Position(eV) | Linewidth(eV) | Integrated Intensity |
|---|---|---|---|---|
| 10 | 4.10 | 0.88 | - | - |
| 30 | 5.80 | 0.87 | - | - |
| 60 | 8.30 | 0.86 | - | - |
| 100 | 9.15 | 0.86 | - | - |
| 300 | 14.25 | 0.86 | - | - |

Possible additional peaks at 1.028 eV, 1.003 eV, and 0.78 eV The presence of these additional peaks makes it difficult to determine linewidth.

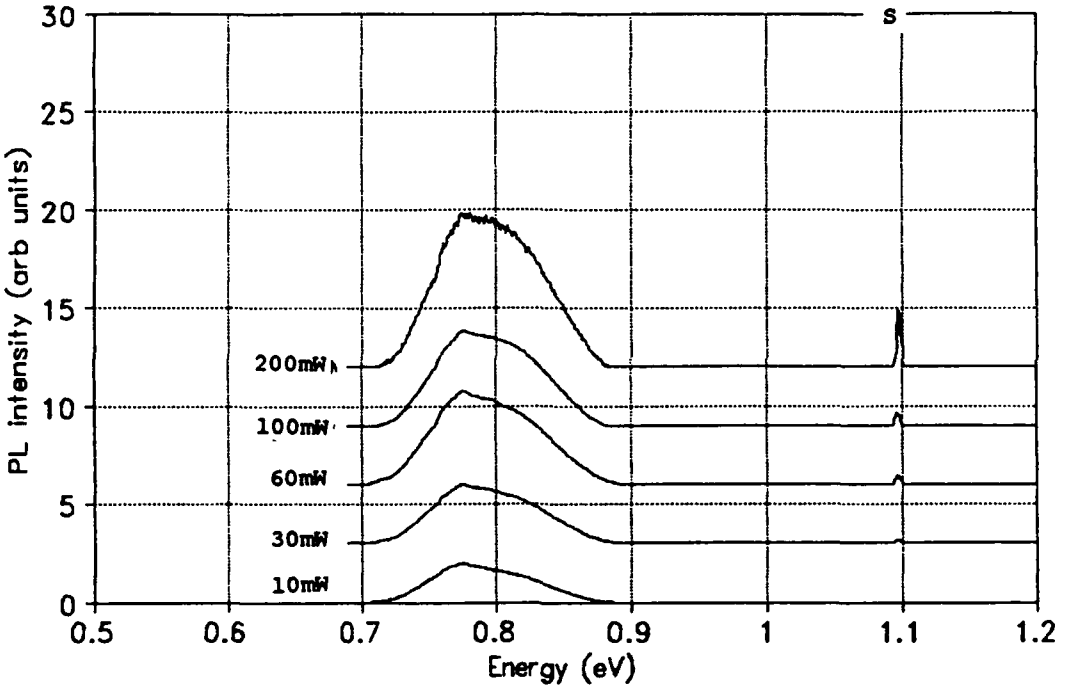


Fig. 30. Broad Energy Luminescence Spectra of Sample 405.1

Sample ID: 405.1
Well Width/Barrier Width: 40 angstroms/80 angstroms
Number of Periods: Approx. 40
Nominal Ge Concentration x: 0.35

Table 20
Sample 405.1 BEL Luminescence

| Exc Pwr(mW) | Peak Intensity | Peak Position(eV) | Linewidth(eV) | Integrated Intensity |
|---|---|---|---|---|
| 10 | 1.98 | 0.774 | 0.087 | 0.1723 |
| 30 | 3.02 | 0.774 | 0.090 | 0.2718 |
| 60 | 4.75 | 0.774 | 0.092 | 0.4370 |
| 100 | 4.80 | 0.774 | 0.091 | 0.4368 |
| 200 | 7.80 | 0.774 | 0.154 | 1.2912 |

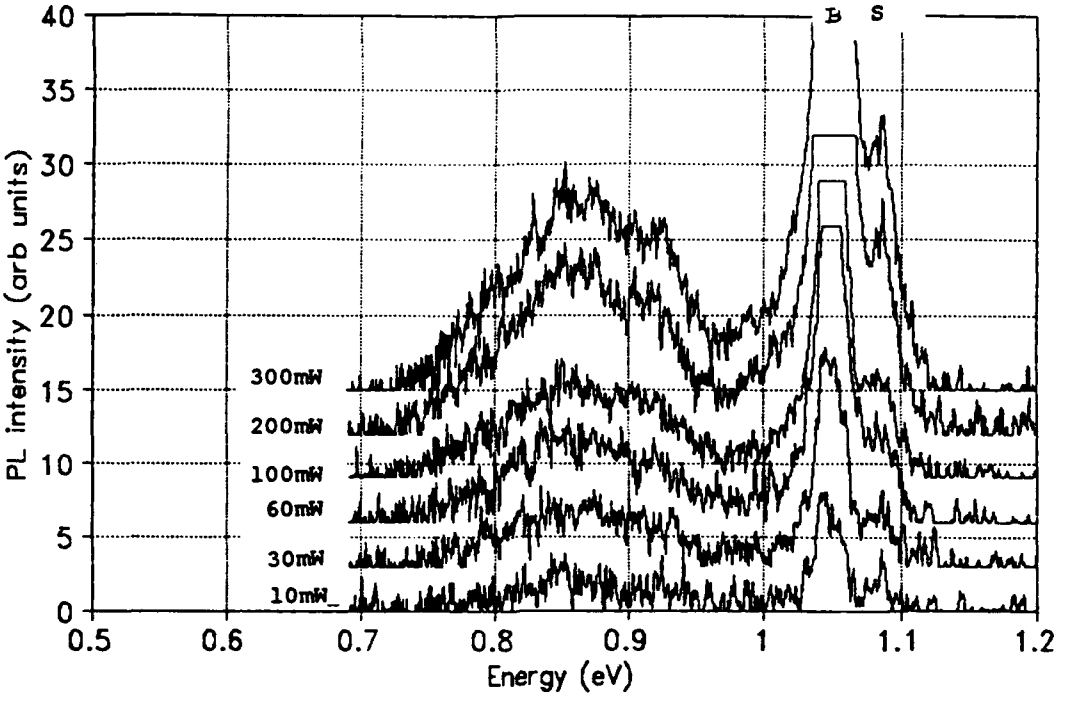


Fig. 31. Broad Energy Luminescence Spectra of Sample 10301.1

Sample ID: 10301.1
Well Width/Barrier Width: 40 angstroms/120 angstroms
Number of Periods: Approx. 30
Nominal Ge Concentration x: 0.25

Table 21
Sample 10301.1 BEL Luminescence

| Exc Pwr(mW) | Peak Intensity | Peak Position(eV) | Linewidth(eV) | Integrated Intensity |
|---|---|---|---|---|
| 10 | 2.90 | 0.850 | - | - |
| 30 | 4.20 | 0.875 | - | - |
| 60 | 5.61 | 0.855 | - | - |
| 100 | 6.50 | 0.860 | - | - |
| 200 | 11.20 | 0.860 | - | - |
| 300 | 12.95 | 0.865 | - | - |

Possible additional peaks at 0.925 and 0.824 eV. The presence of these additional peaks and the unusually large amount of noise make it difficult to determine linewidth.

Fig. 32-34 show plots of the peak intensity versus excitation power for the three samples. As one can see from these plots, the intensity increases linearly with laser power up to 60 mW, then begins to show a sublinear dependence. The peak that Lai and Klein studied also showed a linear power dependence, then a sublinear dependence at higher excitation levels. The explanation may be a saturation[53:3220-1]. The potential wells form bound excitons by first trapping an electron, then attracting a hole by Coulomb force, or vice versa. The rate of bound exciton formation depends on how many of unfilled potential wells there are. At low excitation power levels, there are enough unfilled traps available to capture electrons and holes. The bound exciton formation time is short, and the intensity depends on the number of free charges which in turn depends linearly on the excitation power. At higher powers, there are many free charges and relatively few unfilled traps, and the formation time for bound excitons is long; hence the intensity increases more slowly with laser power.

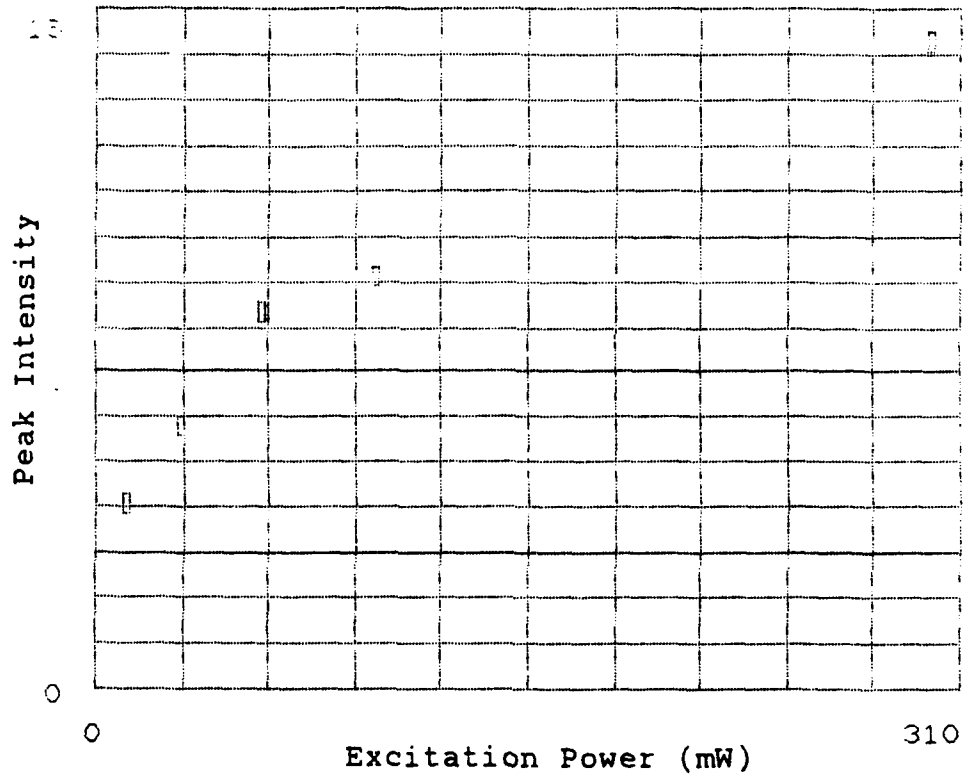


Fig. 32. Sample 326.1 BEL Intensity Versus Excitation Power.

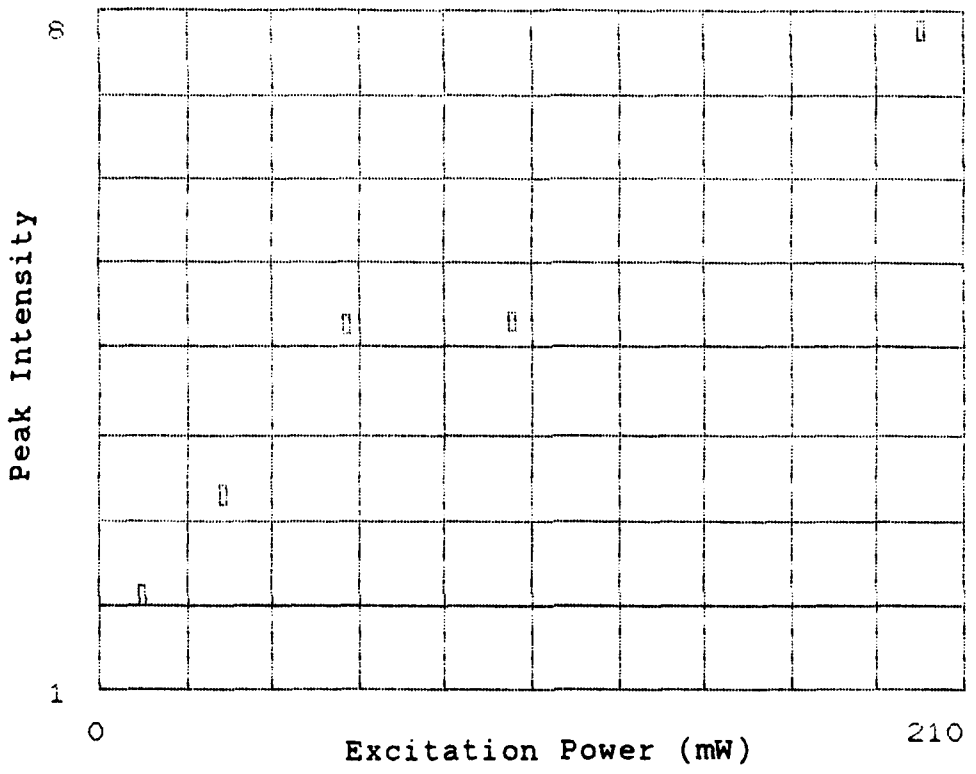


Fig. 33. Sample 405.1 BEL Intensity Versus Excitation Power.

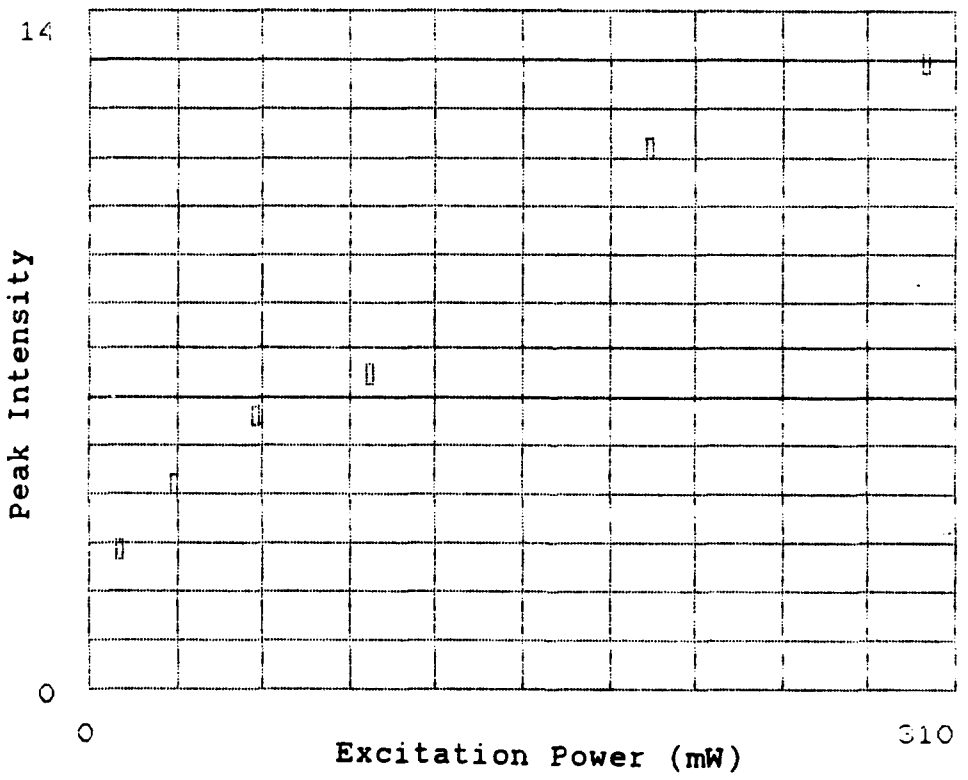


Fig. 34. Sample 10301.1 BEL Intensity Versus Excitation Power.

Fig. 35 shows the effect of annealing temperature on sample 10322.2. The sample was annealed for 30 sec by the RTA method at the temperatures indicated. At higher temperatures the BEL peak showed a pronounced decrease in linewidth, a rise in intensity, and a shift from 0.945 to 0.96 eV. Annealing redistributes the alloy atoms, and in this case seemed to remove most of the deep potential wells. More charge carriers cluster into the remaining wells around 0.96 eV, hence the peak intensity increases around that energy.

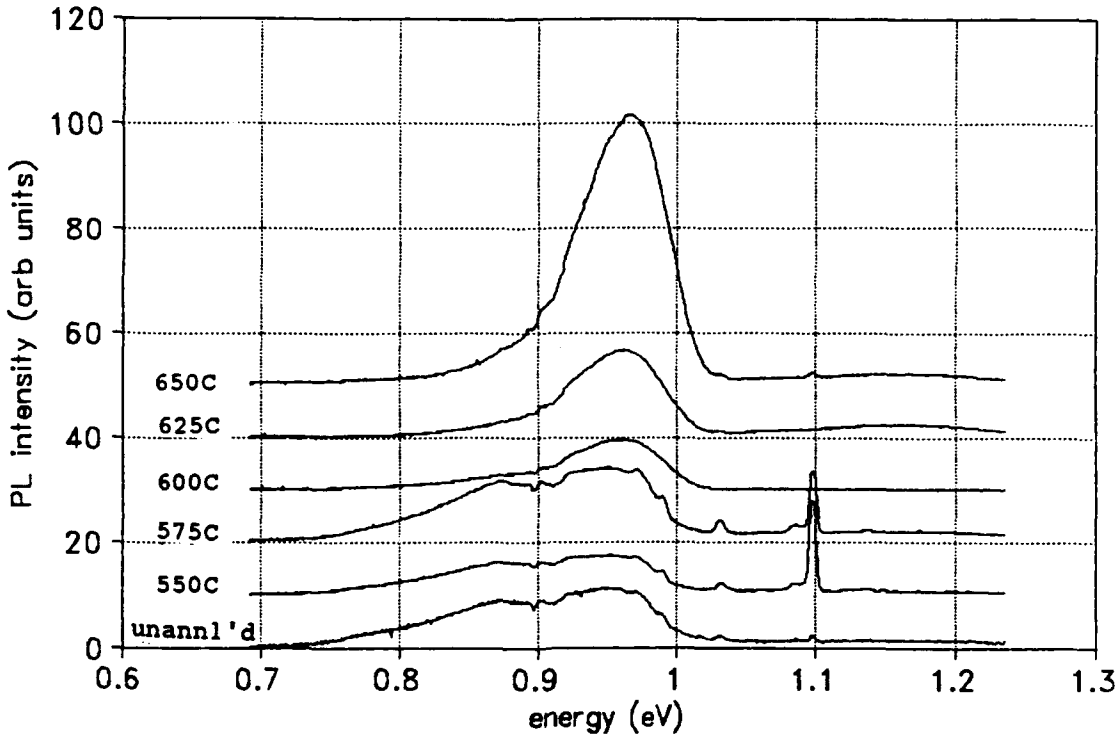


Fig. 35. Sample 10322.2 Annealing Temperature Dependence.

## VII. Conclusions and Recommendations for Future Study

### Part 1

Conclusions:

Si-Ge alloy SLs show strong near-band edge luminescence which is very similar to bulk alloy emissions. No-phonon lines, as well as alloy-related phonon replicas, are visible. The lines vanish at around 15 K. The temperature dependence indicates an activation energy of around 5 meV. This energy and the lines' positions indicate they arise from impurity-bound excitons in the alloy, possibly P, B, or As, as those are common residual impurities in MBE-grown Si[58:359]. The peaks show linewidth broadening, as well as a slight shift to lower energy at higher temperatures. These are caused by alloy composition fluctuations.

Recommendations:

First, PL studies could be made of high quality samples with varying well widths, especially below 20 angstroms, to find the dependence of binding energy on well width for Si-Ge SLs. Second, higher Ge concentration samples could be studied. In particular, in a strained alloy the bandgap changes to Ge-like at x=0.85; do the peak locations and binding energies change sharply at this concentration? These measurements would be made with intentionally-doped samples, for which the well width and nominal alloy concentrations were accurately known. Also, electroreflectance measurements could be used on the samples

studied here and others. These techniques enable one to observe all the optical transitions that occur between the conduction and valence band instead of only the lowest energy transitions. Zeeman measurements, made by splitting the levels with a magnetic field, would indicate more details on the energy structure. Finally, the electrical properties of SLs were not investigated in this project. What are the effects of strain, well width, and Ge concentration on the electron mobility and conductivity?

Part 2

Conclusion:

The broad luminescence is caused by excitons bound to alloy fluctuations. While no definitive proof has been offered that this is true, the data available at least appear to be consistent with such a scenario. No other common transitions in semiconductors or SLs account for all of the peak's properties. The fact that a similar peak has been observed in bulk alloys would seem to rule out strain and SL effects, such as zone-folding, as the cause.

Recommendations:

Perform PL on Ge-doped Si, and compare the spectra with the BEL peak. This would determine whether the BEL is related to isoelectronic center transitions, which it most closely resembles. Also, annealing studies should be done on more samples, and at higher temperatures. In particular, at sufficiently high annealing temperatures the BEL peak is expected

to disappear and dislocations to set in as the alloy strain relaxes. PL with varying laser wavelengths, as well as cathodoluminescence, should be performed. These would indicate the effect on the peak of varying the penetration depth. Electroluminescence could also be done, to find if the luminescence spectra and power dependence resemble those of PL. Finally, samples with higher Ge concentrations should be tested. In Ge-rich alloys the peak should not appear, since local concentrations of Si would create potential hills instead of wells and thus not confine charge carriers. Local regions of pure Ge in the Ge-rich alloy would create small potential wells, but not deep enough to bind significant numbers of excitons at high temperatures.

## Appendix A

In Fig. 18-26, the W-shaped dip at around 0.9 eV is caused by water absorption. The absorption of the sample luminescence occurs between the sample chamber and spectrometer, and inside the spectrometer. Unfortunately, the top of the BEL peak is also in this vicinity for many of the samples. To aid in identifying the peak location and height, a system calibration was performed.

(1) A 1000°C blackbody source was directed at the entrance slit of the spectrometer.

(2) The system output between 1000 and 1800 nm was recorded, using the same sampling software as for data collection.

(3) For each sample point, the system output was divided by the input signal to obtain the system responsivity. The input signal was the Planck blackbody spectrum at each wavelength.

(4) Each sample spectrum was then divided by this responsivity to obtain the original sample luminescence.

(5) Finally, each sample spectrum was smoothed, by replacing each data point by the average of the 10 surrounding points. This served to remove larger noise spikes and fluctuations.

Two GW-BASIC programs were written, one to find the system responsivity and the other to perform the smoothing. The figures on the following pages show the results of this process. The blackbody response was recorded by José Colon and Todd Steiner.

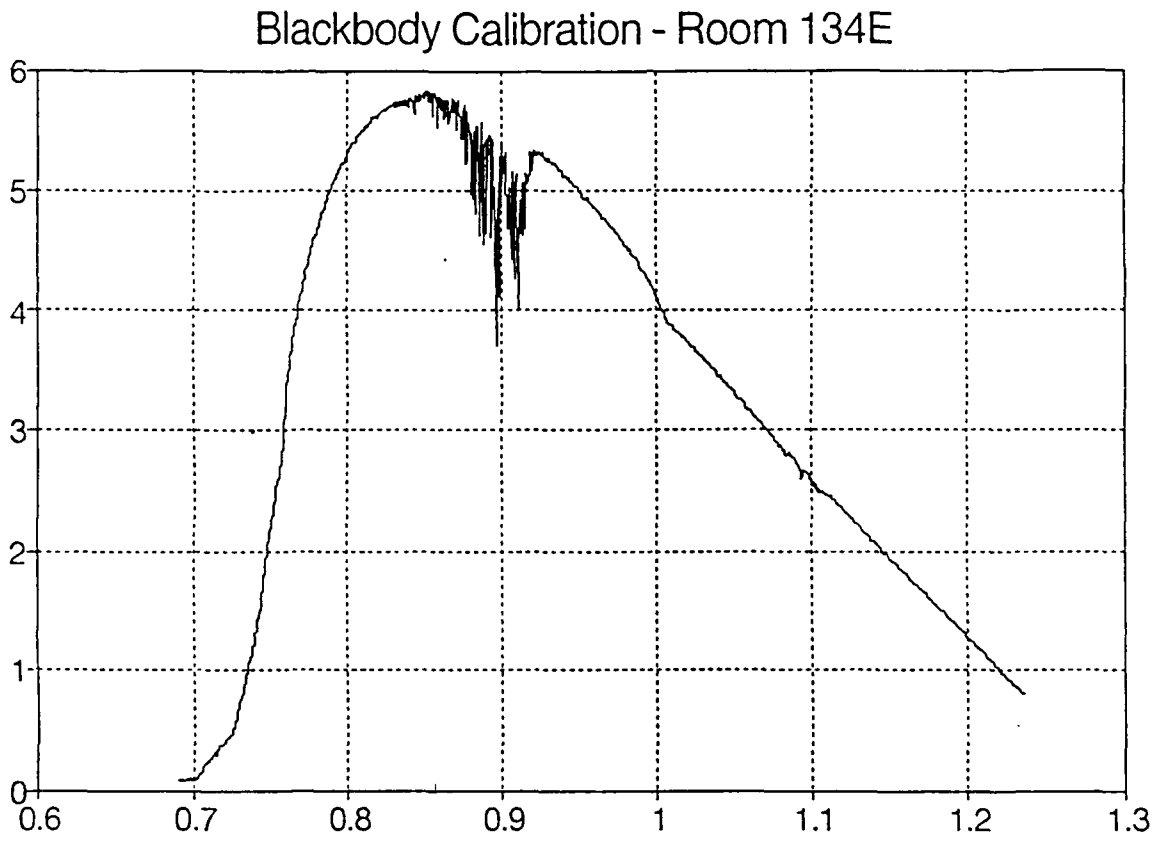


Fig. A1. System Blackbody Response.

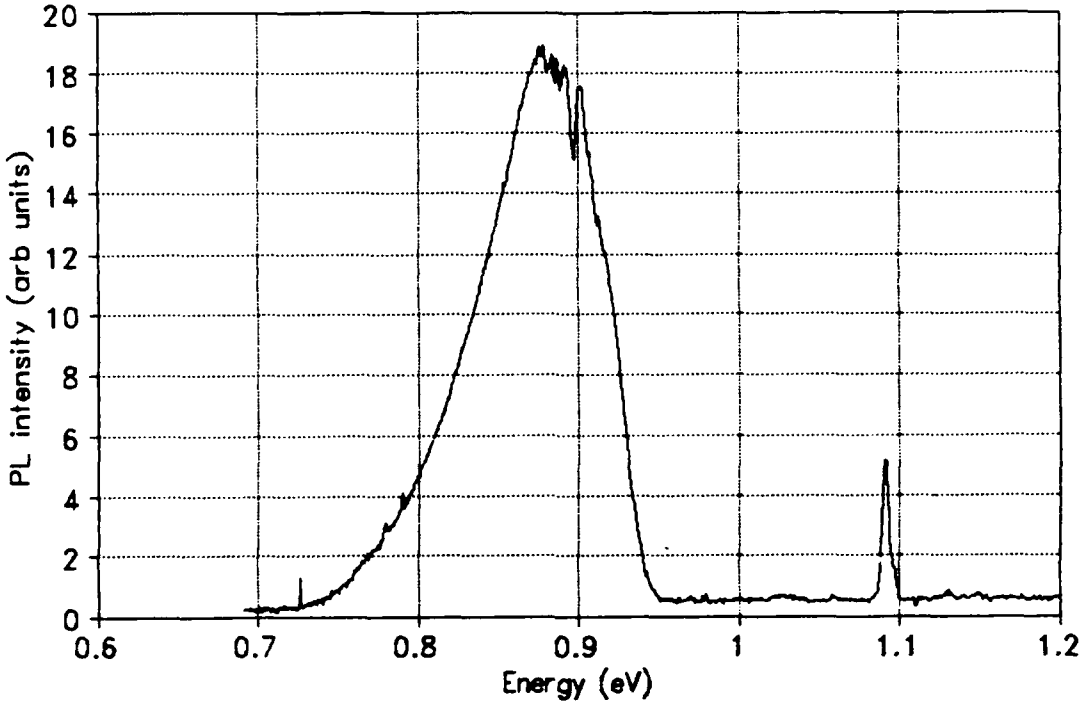


Fig. A2. System Calibration. Spectrum of sample 10531.1 (a) before calibration

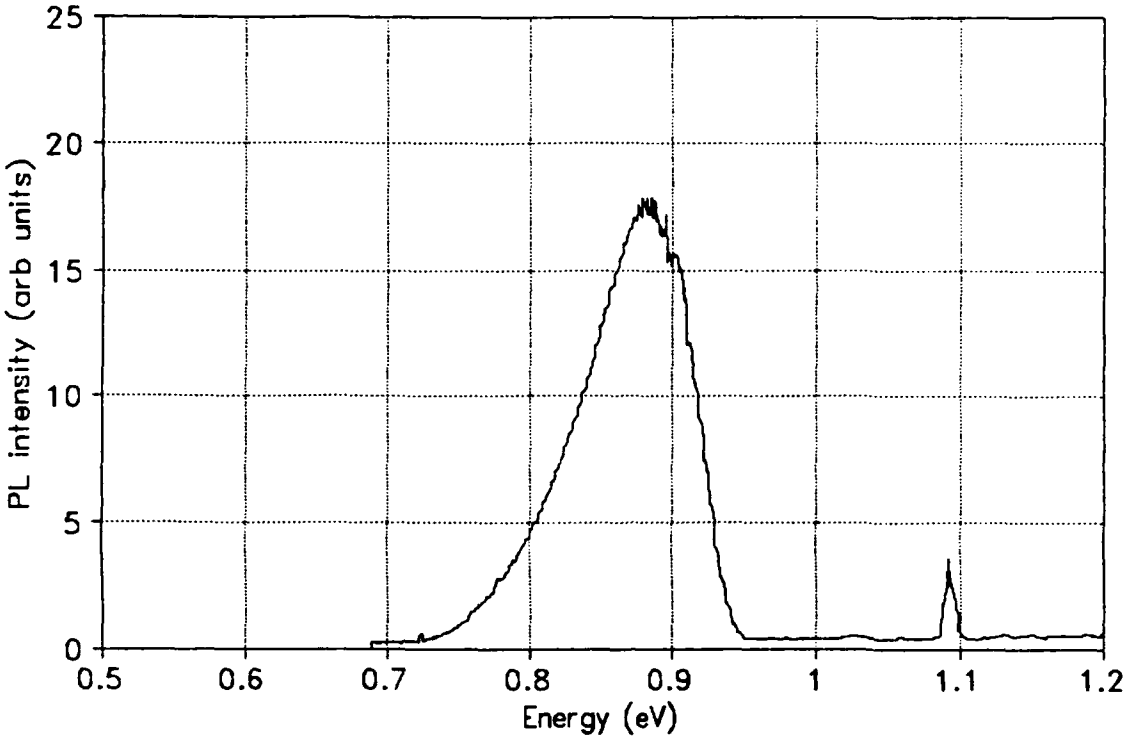


Fig. A3. System Calibration. Spectrum of sample 10531.1 (b) after calibration.

## Appendix B

To demonstrate fluctuations of Ge concentration in a Si-Ge alloy, which is the proposed basis for the BEL peak, a computer program was written to simulate distribution of atoms in a cubic crystal lattice, 20 units on a side. The program:

(1) Distributes an atom at each point in the lattice. The probability of a Si is 75 percent, and of a Ge is 25 percent. The program uses a random number generator to determine which type of atom is placed at each point.

(2) Forms a cube 5 units on a side and moves it to random locations within the lattice (5 units in an Si lattice is roughly equivalent to 12 angstroms, the size of the most effective alloy fluctuations found in Part 2). For each cube location, the fraction of Ge atoms inside the cube is determined and compared to the nominal Ge concentration of 25 percent.

Fig. B1 on the next page shows the result of placing the cube at 30 random locations in the lattice. Note that even for a 20x20x20 lattice, the Ge fluctuation is considerable For the samples studied in this project, the alloy was typically $10^7$ x $10^7$ x 500 units. Fig. B2 shows random placement of "Ge atoms" and "Si atoms" in a 20x20, two-dimensional lattice.

The basic idea for these programs was suggested by Todd Steiner.

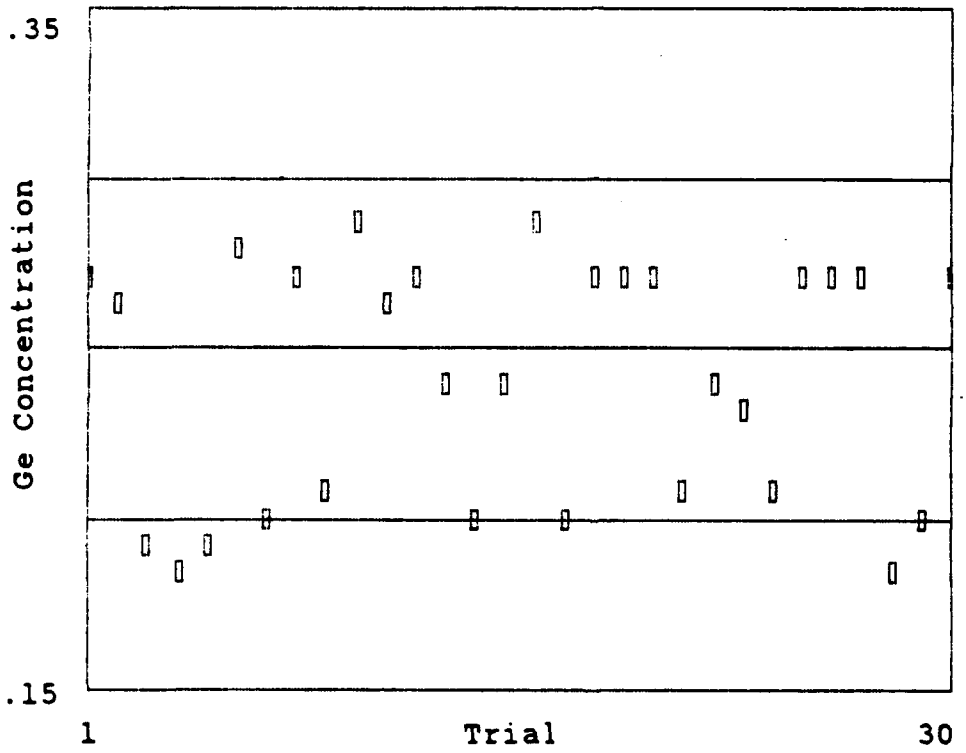


Fig. B1. Local Ge concentration in a 20x20x20 lattice.

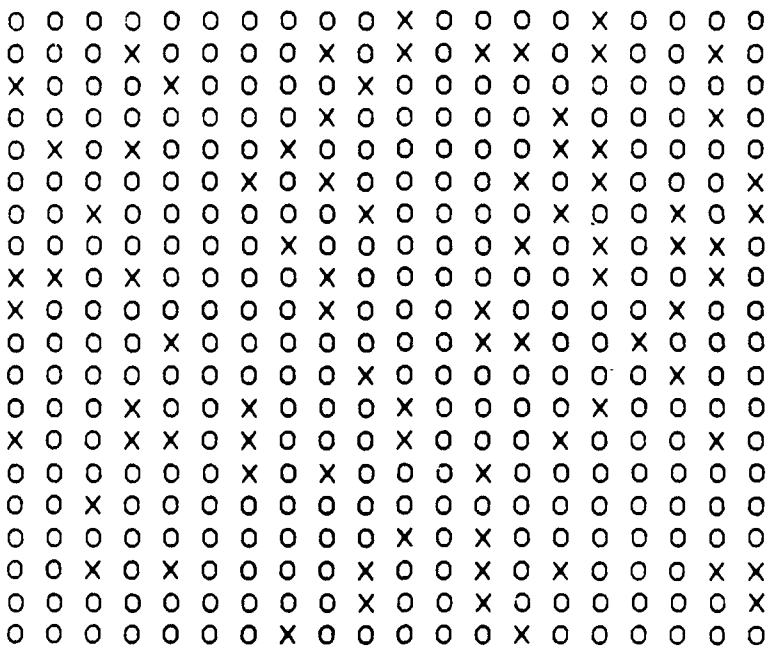

Fig. B2. Placement of Atoms in a Two-Dimensional Lattice. (X=Ge; O=Si)

References

1. Esaki, L. "The Evolution of Quantum Structures," J. de Physique C5-1 (Nov 1987).

2. Temkin, H. et al. "$Ge_xSi_{1-x}$ Strained-Layer Superlattice Waveguide Photodetectors Operating Near 1.3 μm," Appl. Phys. Lett. 48: 463 (14 Apr 1986).

3. Kelly, M.J. "Quantum Semiconductor Devices," Sci. Prog. Oxf. 72: 99-116 (Spring 1988).

4. Ashcroft, N. and N. Mermin. Solid State Physics. Philadelphia: Saunders College, 1976.

5. Smith, R.A. Semiconductors (Second Edition). Cambridge: Cambridge Univ. Press, 1978.

6. Pankove, J. Optical Processes in Semiconductors. New York: Dover, 1971.

7. Eisberg, R. and R. Resnick. Quantum Physics. New York: Wiley, 1974.

8. Davies, G. "The Optical Properties of Luminescence Centres in Silicon," Physics Reports 176: 83-188 (May 1989).

9. Pearsall, T. "Silicon-Germanium Alloys and Heterostructures: Optical and Electronic Properties," CRC Critical Reviews in Solid State and Materials Sciences 15: 551-601 (1989).

10. Abstreiter, G. et al. "Optical and Electronic Properties of Si/SiGe Superlattices," in Two-Dimensional Systems: Physics and New Devices, edited by G. Baver et al. Berlin: Springer, 1986.

11. Abstreiter, G. et al. "Silicon/Germanium Strained Layer Superlattices," J. of Cryst. Growth 95: 431-438 (July 1989).

12. Weisbuch, C. and B. Vinter. Quantum Semiconductor Structures: Fundamentals and Applications. New York: Academic Press, 1991.

13. Weisbuch, C. "Optical Properties of Quantum Wells," in Physics and Applications of Quantum Wells and Superlattices, edited by E.E. Mendesz and K. von Klitzing. NATO ASI, Series B: Physics Vol. 170. New York: Plenum, 1987.

14. Miller, R.C. and D.A. Kleinman. "Excitons in GaAs Quantum Wells", J. of Lumin. 30: 520-540 (1985).

References cont'd

15. Singh, R. "Rapid Isothermal Processing," J. Appl. Phys. 63: R59-R114 (15 April 1988).

16. Davies, G. and D. Williams. "III-V MBE Growth Systems," in The Technology and Physics of Molecular Beam Epitaxy, edited by E.H.C. Parker. New York: Plenum, 1985.

17. Ota, Y. "Silicon Molecular Beam Epitaxy," Thin Solid Films 106: 3-136 (August 12, 1983).

18. Mailhiot, C. and D. Smith. "Strained-Layer Semiconductor Superlattices," in CRC Critical Reviews in Solid State and Materials Sciences 16: 131 (1990).

19. Kasper, E. "Strained Layer Superlattices," in Physics and Applications of Quantum Wells and Superlattices, edited by E.E. Mendesz and K. von Klitzing. NATO ASI, Series B: Physics, Vol. 170. New York: Plenum, 1987.

20. Van de Walle, C. and R. Martin. "Theoretical Study of Si/Ge Interfaces," J. Vac. Sci. Tech. B3: 1256-1259 (Jul/Aug 1985).

21. Ting, D.Z.-Y. and Y.C. Chang. "Electronic and Optical Properties of Strained-Layer Superlattices Made of Semiconductor Alloys," J. Vac. Sci. Tech. B4: 1002-1005 (Jul/Aug 1986).

22. Gell, M.A. "Effect of Buffer-Layer Composition on New Optical Transitions in Si/Ge Short-Period Superlattices," Phys. Rev. B38: 7535-7540 (15 October 1988).

23. Okumura, H. et al. "Observation of Direct Band Gap Properties in $Ge_nSi_m$ Strained-Layer Superlattices," Japanese J. Appl. Phys. 28: L1893-L1895 (November 1989).

24. Zachai, R. et al. "Photoluminescence in Short-Period Si/Ge Strained-Layer Superlattices," Phys. Rev. Lett. 64: 1055-1058 (26 February 1990).

25. Schmid, U. et al. "Direct Transition Energies in Strained Ten-Monclayer Ge/Si Superlattices," Phys. Rev. Lett. 65: 2610 (12 November 1990).

26. Noel, J.-P. et al. "Intense Photoluminescence Between 1.3 and 1.8 m From Strained $Si_{1-x}Ge_x$ Alloys," Appl. Phys. Lett. 57: 1037-1039 (3 September 1990).

27. Sturm, J.C. et al. "Well-Resolved Band-Edge Photoluminescence of Excitons Confined in Strained $Si_{1-x}Ge_x$ Quantum Wells," Phys. Rev. Lett. 66: 1362-1365 (11 March 1991).

References cont'd

28. Davies, G. "The Optical Properties of Luminescence Centers in Silicon," Physics Reports 176: 83-188 (May 1989).

29. Sauer, R., J. Weber, and J. Stolz. "Dislocation-Related Photoluminescence in Silicon," Appl. Phys. A36: 1-13 (January 1985).

30. Weber, J., and M.I. Alonso. "Near-Band-Gap Photoluminescence of Si-Ge Alloys," Phys. Rev. B40: 5683-5693 (15 September 1989).

31. Weisburd, S. "Silicon Devices: LED There Be Light," Science News 131: 294-295 (May 9, 1987). {2}

32. Bajaj, K.K., D.C. Reynolds et al. "High-Resolution Photoluminescence Studies of GaAs/GaAlAs Multi-Quantum Well Structures Grown by Molecular Beam Epitaxy," Solid-State Electronics 29: 215-227 (February 1986).

33. Masselink, W.T. et al. "Shallow Impurity Levels in AlGaAs/GaAs Semiconductor Quantum Wells," Solid-State Electronics 29: 205-214 (February 1986).

34. Weisbuch, C. "Fundamental Properties of III-V Semiconductor Two-Dimensional Quantized Structures: The Basis for Optical and Electronic Device Applications," in Semiconductors and Semimetals, Vol. 24: Applications of Multiquantum Wells, Selective Doping, and Superlattices edited by R. Dingle. New York: Academic Press, 1987.

35. Mitchard, G.S. and T.C. McGill. "Photoluminescence of Si-Rich Si-Ge Alloys," Phys. Rev. B25: 5351-5363 (15 April 1982).

36. Schubert, E.F. et al. "Alloy Broadening in Photoluminescence Spectra of $Al_xGa_{1-x}As$," Phys. Rev. B30: 813-820 (15 July 1984).

37. Modavis, R.A. and D.G. Hall. "Aluminum-Nitrogen Isoelectronic Trap in Silicon," J. Appl. Phys. 67: 545-547 (1 January 1990).

38. Bradfield, P.L., T.G. Brown, and D.G. Hall. "Radiative Decay of Excitons Bound to Chalcogen-Related Isoelectronic Impurity Complexes in Silicon," Phys. Rev. B38: 3533-3536 (15 August 1988).

39. Brown, T.G. and D.G. Hall. "Optical Emission at 1.32 μm from Sulfur-Doped Crystalline Silicon," Appl. Phys. Lett. 49: 245-247 (4 August 1986).

References cont'd

40. Lightowlers, E.C. and G. Davies. "Spectroscopy of Excitons Bound to Isoelectronic Defect Complexes in Silicon," Solid State Comm. 53: 1055-1060 (March 1985).

41. Henry, M.O. et al. "Bound Exciton Recombination in Beryllium-Doped Silicon," J. Phys. C14: L255-L261 (15 January 1981).

42. Weber, J., W. Schmid, and R. Sauer. "Localized Exciton Bound to an Isoelectronic Trap in Silicon," Phys. Rev. B21: 2401-2414 (15 March 1980).

43. Mitchard, G.S. et al. "Observation of Long Lifetime Lines in Photoluminescence From Si:In," Solid State Comm. 29: 425-429 (February 1979).

44. Modavis, R.A. et al. "Isoelectronic Bound Exciton Emission from Si-Rich Silicon-Germanium Alloys," Appl. Phys. Lett. 57: 954-956 (3 September 1990).

45. Guillaume, C.B. and M. Voos. "Electron-Hole Drops in Ge-Si Alloys," Phys. Rev. B10: 4995-5001 (15 December 1974).

46. Schowalter, L.J. et al. "Long Lifetimes of Excitons in Stressed Ge," Solid State Comm. 37: 319-324 (January 1981).

47. Schowalter, L.J. et al. "Evidence for Separate Mott and Liquid-Gas Transitions in Photoexcited Strained Germanium," Phys. Rev. B 29: 2970-2985 (15 March 1984).

48. Alferov, Zh.I., E.L. Portnoi, and A.A. Rogachev. "Width of the Absorption Edge of Semiconducting Solid Solutions," Sov. Phys. Semicond. 2: 1001-1003 (February 1969).

49. Baranovskii, S.D. and A.L. Efros. "Band Edge Smearing in Solid Solutions," Sov. Phys. Semicond. 12: 1328-1330 (November 1978).

50. Reif, F., Fundamentals of Statistical and Thermal Physics. New York: McGraw-Hill, 1965.

51. Lai, S. and M.V. Klein. "Evidence for Exciton Localization by Alloy Fluctuations in Indirect-Gap $GaAs_{1-x}P_x$," Phys. Rev. Lett. 44: 1087-1090 (21 April 1980).

52. Lang, D.V. et al. "Measurement of the Band gap of $Ge_xSi_{1-x}$/Si Strained-Layer Heterostructures," Appl. Phys. Lett. 47: 1333-1335 (15 December 1985).

References cont'd

53. Lai, S.T. and M.V. Klein. "Photoluminescence Study of Excitons Localized in Indirect-Gap $GaAs_{1-x}P_x$," Phys. Rev. B29: 3217-3224 (15 March 1984).

54. Burns, G. Solid State Physics. New York: Academic Press, 1985.

55. Pikhtin, A.N. "Optical Transitions in Semiconducting Solid Solutions (Review)," Sov. Phys. Semicond. 11: 245-264 (March 1977).

56. Gnutzmann, U. and K. Clausecker. "Theory of Direct Optical Transitions in an Optical Indirect Semiconductor with a Superlattice Structure," Appl. Phys. 3: 9-14 (January 1974).

57. Rajakarunanayake, Y. and T.C. McGill. "Strain Effects and Optical Properties of $Si_{1-x}Ge_x$/Si Superlattices," J. Vac. Sci. Tech. B7: 799-803 (July/August 1989).

58. Shiraki, Y. "Silicon Molecular Beam Deposition," in The Technology and Physics of Molecular Beam Epitaxy, edited by E.H.C. Parker. New York: Plenum Press, 1985.